This is a repository copy of *High voltage coefficient piezoelectric materials and their applications*.

White Rose Research Online URL for this paper:
https://eprints.whiterose.ac.uk/175888/

Version: Accepted Version

Article:

High Voltage Coefficient Piezoelectric Materials and Their Applications

Thomas E. Hooper[a]*, James. I. Roscow[b], Andrew Mathieson[c], Hamideh Khanbareh[b], Anton J. Goetzee-Barral[a] & Andrew J. Bell[a]

[a]School of Chemical and Process Engineering, University of Leeds, Leeds LS2 9JT, UK
[b]Department of Mechanical Engineering, University of Bath, Bath BA1 9BJ, UK
[c]Ultra Maritime Systems, Dartmouth, Nova Scotia Canada, B2Y 4N2

Abstract

The piezoelectric d_{ij} coefficient is often regarded in materials science as the most important figure of merit of piezoelectric performance. For many applications, the piezoelectric g_{ij} coefficient which correlates to voltage output and sensitivity of a piezoelectric material can be considered of equal or increased importance, is often an overlooked parameter in materials science literature. The aim of this review is to highlight the importance of this parameter and to provide insight into the mechanisms that drive a high piezoelectric voltage coefficient in single crystal, polycrystalline, and composite form. For bulk ceramics, special attention is given to tetragonal systems due to the availability of electrical and crystallographic data allowing for a clear structure-property relation. Orthorhombic and rhombohedral systems are mentioned and specific cases highlighted, however investigating structure-property relations is difficult due to the lack of crystallographic datasets. Composite materials have been the forefront of high g_{ij} piezoelectric materials over the decades and are therefore also considered in both ceramic-matrix and polymer-matrix form. An overview of applications in medical, energy, fishing and defence industries where a high g_{ij} is desirable are considered and the scientific and commercial considerations that must be made for the transition from laboratory to industry are discussed from the perspective of integrating new piezoelectric materials into sonar devices.

Keywords: piezoelectric, ferroelectric, piezovoltage, single crystal, polycrystalline, piezocomposites, applications

---

*Corresponding author: t.e.hooper@leeds.ac.uk

1   Introduction

The ability for piezoelectric materials to convert mechanical energy into electrical energy and vice versa has resulted in them being exploited in devices for many decades [1-4]. Other advantages such as high electromechanical coupling coefficients (k_{33} = 0.1-0.9), a wide range of permittivities (ε_r = 100-3000), low dielectric and mechanical losses as well as high thermal stability are also realised. Perhaps the most important figure of merit for piezoelectric performance is the electromechanical coupling coefficient, k_{ij}, which represents the amount of converted mechanical (electrical) energy into electrical (mechanical) energy per total input energy [4]. Despite this, the most often cited figure of merit for a piezoelectric material is the piezoelectric charge coefficient, d_{ij}, which represents the change in polarisation per unit stress (C/N) for the direct effect or the amount of strain developed per unit field (m/V) for the converse effect. Polycrystalline lead zirconate titanate (Pb(Zr,Ti)O$_3$ or PZT) has been the cornerstone of piezoelectric devices due to its high performance and versatility through doping and compositional variation with some compositions reaching d_{33} values of ≈750pC/N [5].

Over the past few decades the development and commercial availability of high performance piezoelectric single crystals with d_{33} values of ≈2000pC/N have revolutionised military and medical applications [6-9]. For some applications, a high voltage output and/or increased sensitivity to perturbation is of equal or increased significance and achieved using materials possessing a large piezoelectric voltage coefficient, g_{ij}, which presents the electric field produced per unit stress for the direct effect, or the strain produced per unit change in polarisation for the converse effect. The relationship between the charge coefficient and the voltage coefficient is analogous to the fundamental circuit equation V = Q / C as shown in Equations 1-4, where V is voltage, Q is charge, C is capacitance which in the case of piezoelectric materials is represented through the permittivity, ε_{ij}.

$$g_{33} = \frac{d_{33}}{\varepsilon_{33}^T \varepsilon_0} \tag{1}$$

$$g_{31} = \frac{d_{31}}{\varepsilon_{33}^T \varepsilon_0} \tag{2}$$

$$g_{15} = \frac{d_{15}}{\varepsilon_{11}^T \varepsilon_0} \tag{3}$$

$$g_h = \frac{d_h}{\varepsilon_{33}^T \varepsilon_0} \tag{4}$$

Where d_{33}, d_{31}, d_{15}, and d_h are the longitudinal, lateral, shear and hydrostatic charge coefficients, ε_{33}^T and ε_{11}^T are the parallel and perpendicular components of the permittivity at constant tensile stress, and ε_0 is the permittivity of free space. Whilst the relationship between the piezoelectric charge and

voltage coefficient suggest that high performance PZT and piezoelectric single crystals also result in high g_{ij}, an increase in d_{ij} is often coupled with an increase in permittivity and therefore the g_{ij} coefficient remains relatively constant in these materials as shown in Figure 1.
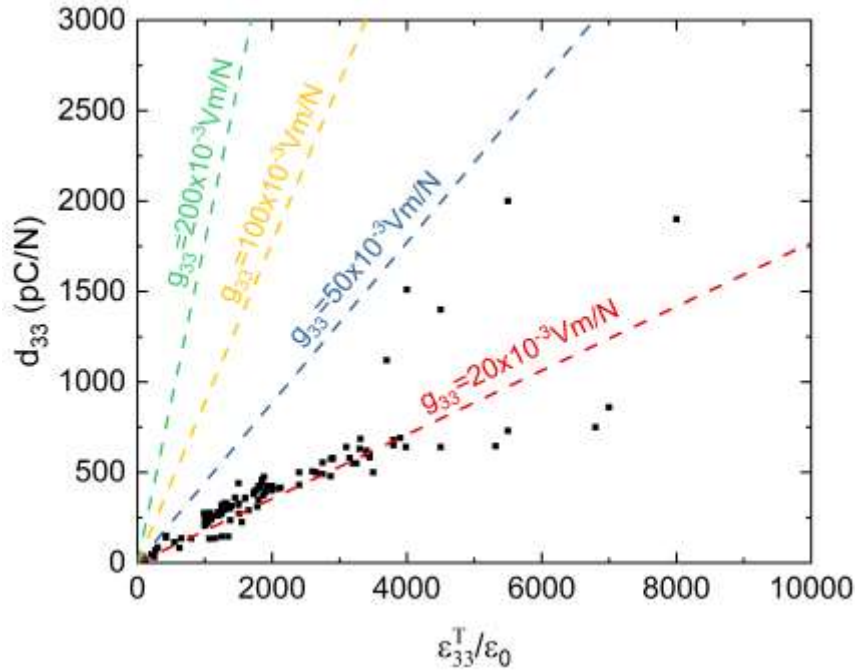

Figure 1: Piezoelectric d_{33} coefficient vs. relative permittivity for a range of commercially available polycrystalline and single crystal materials. All datapoints taken from supplementary data in Ref. [10], except values for Generation II and III single crystals which are taken from Ref. [7]

Despite Figure 1 suggesting a fundamental cap to g_{33} due to d_{33}-ε_{33}^T coupling, significant advancements in processing capabilities, the development of new materials and tuning of current materials either compositionally or through doping has resulted in the successful enhancement of the voltage coefficient. For the sake of this review, 'bulk' ceramics will encompass single crystal, polycrystalline and textured ceramics, whereas 'composite' ceramics will be used to define ceramic-matrix and polymer-matrix composites.

This review is split into parts allowing for selective access by the reader. Section 2, 3 and 4 evaluates the g_{ij} coefficient in single crystals, polycrystalline and textured ceramic form, respectively. Initially the voltage coefficient is analysed from a mathematical perspective using Landau-Devonshire theory, before exploring electrical and crystallographic data from literature and proposing structure-property relations. Potential scientific and industrial issues associated with the commercialisation of these materials, particularly single crystals, are also discussed. Section 5 discusses the g_{ij} coefficient in both ceramic-composite (5.1) and polymer-composite form (5.2) and the influence of composite structure, volume fraction and processing are considered. Section 6 moves away from materials science and discusses

the importance of this parameter in three applications: polymer-matrix sensors (6.1), energy harvesters (6.2) and sonar (6.3). Section 7 discusses the additional safety and commercial considerations that must be made for the successful transition of new piezoelectric materials into industry from the perspective of sonar applications. Finally, section 8 summarises the findings of this review, provides insight into the potential 5-year growth of the piezoelectric device market, and highlights potential research avenues that may arise in order to meet this commercial demand.

2   Single Crystals & Single Domain Systems

The Landau-Devonshire [11, 12] derived g_{ij} coefficients for a ferroelectric perovskite in the tetragonal, orthorhombic and rhombohedral phases are shown in Equation 5-7.

$$\text{Tetragonal} \begin{pmatrix} 0 & 0 & 0 & 0 & Q_{44}P_3 & 0 \\ 0 & 0 & 0 & Q_{44}P_3 & 0 & 0 \\ 2Q_{12}P_3 & 2Q_{12}P_3 & 2Q_{11}P_3 & 0 & 0 & 0 \end{pmatrix} \tag{5}$$

$$\text{Orthorhombic} \begin{pmatrix} 0 & 0 & 0 & 0 & Q_{44}P_3 & Q_{44}P_2 \\ 2Q_{12}P_2 & 2Q_{11}P_2 & 2Q_{12}P_2 & Q_{44}P_3 & 0 & 0 \\ 2Q_{12}P_3 & 2Q_{12}P_3 & 2Q_{11}P_3 & Q_{44}P_2 & 0 & 0 \end{pmatrix} \tag{6}$$

$$\text{Rhombohedral} \begin{pmatrix} 2Q_{11}P_1 & 2Q_{12}P_1 & 2Q_{12}P_1 & 0 & Q_{44}P_3 & Q_{44}P_2 \\ 2Q_{12}P_2 & 2Q_{11}P_2 & 2Q_{12}P_2 & Q_{44}P_3 & 0 & Q_{44}P_1 \\ 2Q_{12}P_3 & 2Q_{12}P_3 & 2Q_{11}P_3 & Q_{44}P_2 & Q_{44}P_1 & 0 \end{pmatrix} \tag{7}$$

Where Q_{ij} are the electrostriction coefficients and P_1, P_2, and P_3 are the orthogonal components of spontaneous polarisation along the [100], [010] and [001] directions. For tetragonal materials, the spontaneous polarisation (P_S) = P_3, whereas for the orthorhombic and rhombohedral phase, $P_2 = P_3 = P_S/\sqrt{2}$ ($P_1 = 0$) and $P_1 = P_2 = P_3 = P_S/\sqrt{3}$, respectively, implying that the most significant g_{ij} values may be observed in tetragonal materials.
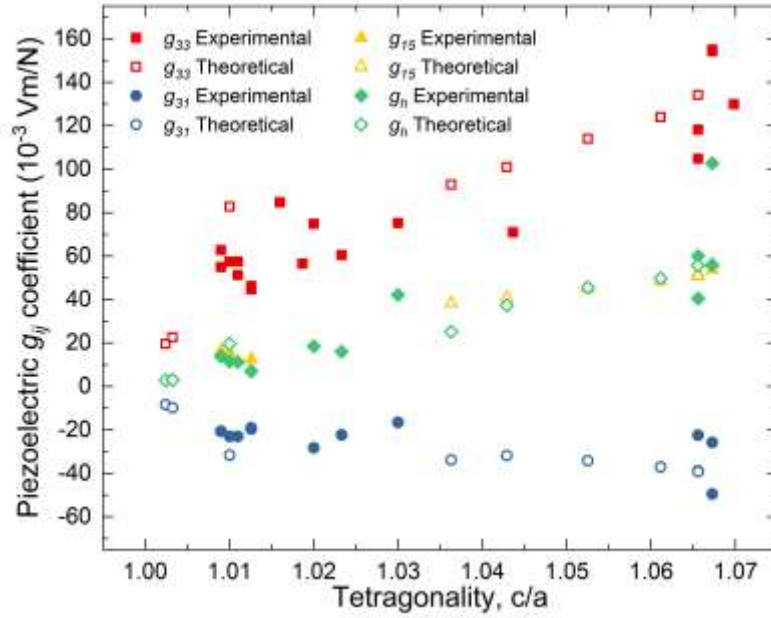
Figure 2: Piezoelectric g_{33}, g_{31}, g_{15} and g_h coefficients as a function of tetragonality, c/a, for *P*4*mm* single crystals throughout literature. Material properties can be found in supplementary material.

When considering tetragonal systems, material properties of crystals are relatively scarce for two reasons. Firstly the drive for high d_{ij} coefficients materials has resulted in the preferred growth of [001] domain engineered rhombohedral crystals, making the motivation for tetragonal crystal growth low. Secondly the large spontaneous strain of tetragonal materials particularly materials exceeding 1% results in processing difficulties, with samples often displaying significant cracking or small sample size limiting characterisation ability. However despite these factors, a structure-property relation can be established for these systems. Figure 2 shows the g_{33}, g_{31}, g_{15} and g_h as a function of tetragonality from experimental and theoretical work of *P*4*mm* single crystals from throughout literature (values can be found in supplementary material). Both the d_{ij} and relative permittivity are heavily dependent on the change in polarisation with electric field, which decreases with tetragonality due to increasing degree of covalency and subsequent decrease in ionic mobility. However the d_{ij} coefficient is also dependent on the absolute value of polarisation ($d_{33} = 2Q_{11}P\varepsilon_{33}$) which increases with tetragonality. Therefore although the piezoelectric charge coefficients and relative permittivity both decrease with tetragonality, it is the faster rate of decay in relative permittivity that results in an enhancement of the g_{ij} coefficient. The increase in tetragonality also results in an increase in piezoelectric anisotropy as shown in Figure 3, between both the lateral-longitudinal -g_{31}/g_{33} modes resulting in enhanced hydrostatic properties and shear-longitudinal modes g_{15}/g_{33}.
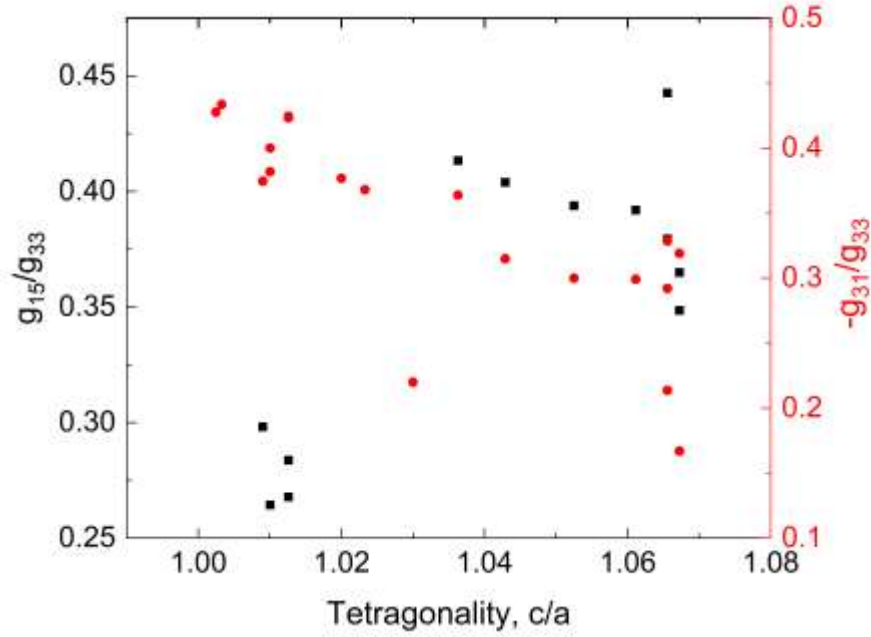
Figure 3: Piezoelectric anisotropy between the shear-longitudinal modes (g_{15}/g_{33}) and lateral-longitudinal ($-g_{31}/g_{33}$) for tetragonal single crystals from literature

It is useful to calculate the piezoelectric properties as a function of angle away from the polar axis to observe whether a ferroelectric material exhibits 'extender' or 'rotator' behaviour. Rotator ferroelectrics arise when the piezoelectric properties are enhanced through the application of an electric field away from the polar axis. These types of ferroelectrics also possess higher d_{15}/d_{33} ratios with the large shear component contributing to d_{31} values which reduces the hydrostatic properties. Extender ferroelectrics possess smaller d_{15}/d_{33} ratios and show the largest d_{33} along the polar axis, and therefore contribution to the d_{31} from the shear component is substantially lower resulting in larger piezoelectric anisotropy and hydrostatic coefficients [13]. If all piezoelectric properties are known, the orientational dependence can be calculated by converting to alternative coordinate systems. The longitudinal charge coefficient (d_{33}^{*}) and relative permittivity ($\varepsilon_{33}^{T*}/\varepsilon_0$) as function of angle away from the polar axis (θ) can be calculated using Equation 8 and 9, respectively.

$$d_{33}^{*} = cos\theta (d_{31} \sin^2 \theta + d_{15} \sin^2 \theta + d_{33} \cos^2 \theta) \tag{8}$$

$$\frac{\varepsilon_{33}^{T*}}{\varepsilon_0} = \left(\frac{\varepsilon_{11}^{T}}{\varepsilon_0}\right) \sin^2 \theta + \left(\frac{\varepsilon_{33}^{T}}{\varepsilon_0}\right) \cos^2 \theta \tag{9}$$

Figure 4 shows the polar plots of (a) d_{33}^{*}, (b) $\varepsilon_{33}^{T*}/\varepsilon_0$, and (c) g_{33}^{*} for varying tetragonalities. The d_{33}^{*} shows clear distinguishability between the rotator and extender behaviour of tetragonal materials and for $\varepsilon_{33}^{T*}/\varepsilon_0$, all materials show a similar trend showing a maximum perpendicular to the polar axis. The dielectric

anisotropy is largest at low tetragonalities which exhibits a more defined 'donut' shape with larger indentation along the polar axis. As tetragonality increases dielectric anisotropy decreases, gradually replacing the well-defined donut shape with an elongated sphere however still showing a maximum perpendicular to the polar axis. Figure 4 shows that whilst the piezoelectric d^*_{33} coefficient clearly distinguishes between extender and rotator ferroelectrics, the piezoelectric g^*_{33} coefficient shows extender ferroelectric behaviour for all tetragonal materials.

Recently Koruza et al. [14] have provided a status on the growth and characterisation of $(K,Na)NbO_3$ single crystals. Although not explicitly mentioned in Ref. [14], when calculated, some orthorhombic systems are found to have significantly large values for the g_{33}, however the compositional variation is vast and not clearly understood. For example $(K_{0.622}Na_{0.378})NbO_3$ single crystals [15] are found to possess g_{33} values of $260x10^{-3}$ Vm/N. However the g_{33} of $(K_{0.538}Na_{0.462})NbO_3$ decreases significantly to $48.3x10^{-3}$ Vm/N as a result of a five-fold increase in the relative permittivity. More studies and datasets are required in order to understand this phenomenon and due to the lack of crystallographic data for orthorhombic single crystals. Furthermore, due to the wide degree of variables such as poling direction and efficiency, domain configurations, and growth techniques, investigating the structure-property mechanisms for these systems is difficult. When the g_{33} is plotted as a function of the individual lattice parameters, lattice parameter ratios and cell volume in both 'pure' orthorhombic and pseudo-monoclinic form (Figure S1 in supplementary data), no correlation can be observed highlighting a more complex relationship compared to a rudimentary rattling ion model adopted for $P4mm$ systems.
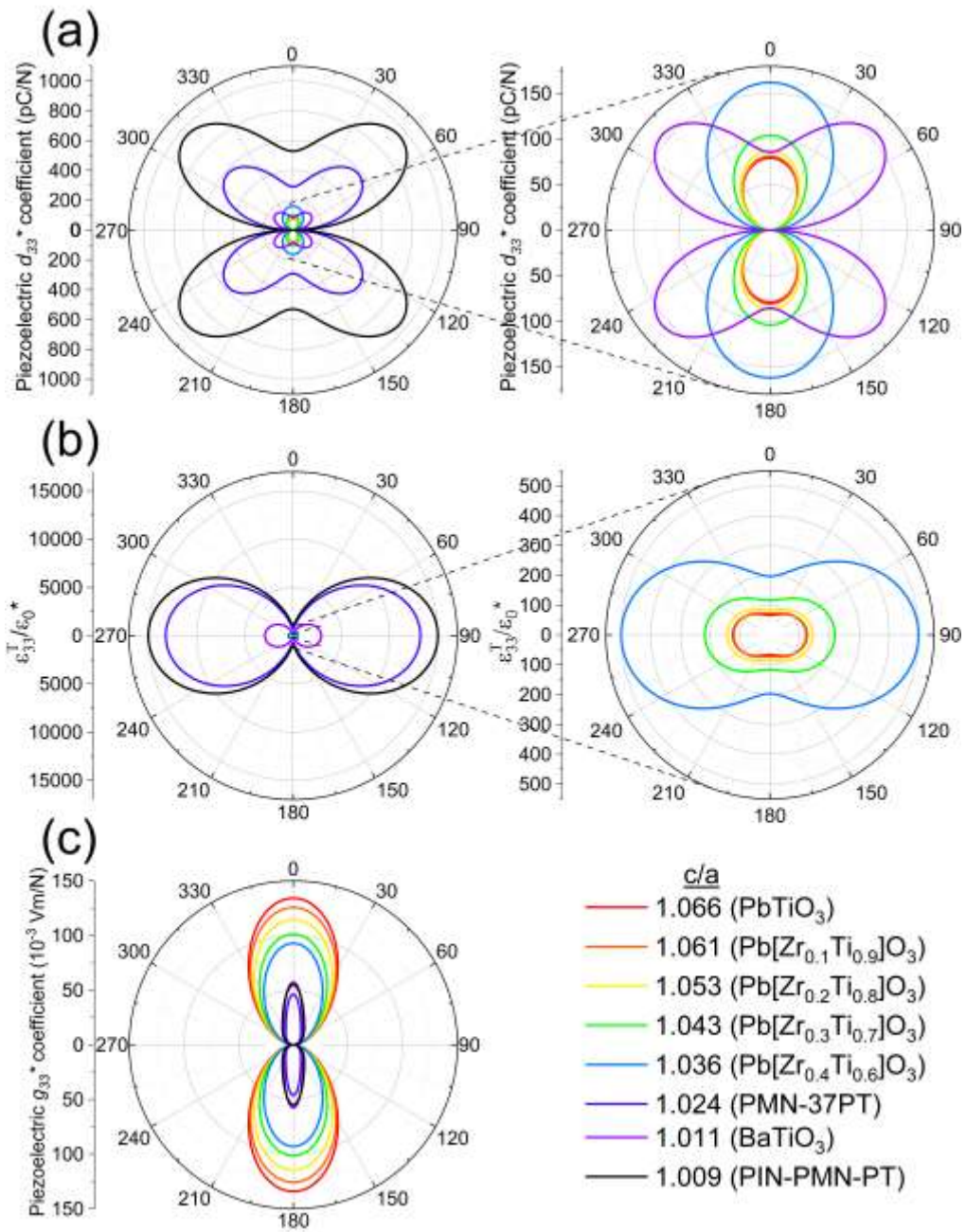
Figure 4: Polar plots of (a) piezoelectric charge coefficient, d_{33}^* (b) relative permittivity, $\varepsilon_{33}^{T*}/\varepsilon_0$, and (c) piezoelectric voltage coefficient, g_{33}^* as a function of angle away from the polar axis. d_{33}^* calculated using Equation 8 and $\varepsilon_{33}^{T*}/\varepsilon_0$ calculated using Equation 9 using piezoelectric and dielectric values for tetragonal single crystals and single domains (material properties found in Supplementary spreadsheet).

Given that the values for the spontaneous polarisation of $KNbO_3$ and $(K,Na)NbO_3$ is less than that of $PbTiO_3$, the large g_{ij} coefficient is potentially facilitated by electrostriction. Using a Leonard-Jones approach to consider the average induced strain and polarisation under an electric field, the electrostriction coefficient, Q_{11}, can be expressed using Equation 10 [16, 17].

$$Q_{11} = \frac{12\zeta r_0^5}{\eta q^2} \tag{10}$$

Where r_0 is the nearest neighbour distance, q is charge and ζ and η represent the anharmonic and harmonic energy components. As the value of Q_{11} can be dictated by ζ/η, it could therefore be that the crystal structure of tetragonal materials results in a more rigid framework where the material behaves more like an ideal harmonic oscillator which in turn increases η and reduces the electrostriction coefficient. This was evidenced by Darlington and Knight [18] who found the electrostrictive deformation of $KNbO_3$ to be around twice that of $BaTiO_3$, concluding that it is "not true to say that the octahedron behaves as a rigid unit moving against other atoms". However the relationship between lattice anharmonicity and piezoelectric voltage coefficients is purely speculative and more research, particularly atomistic modelling, needs to be carried out in order to support or contest this.

Rhombohedral crystals show relatively low values for the piezovoltage coefficient, as suggested by Landau-Devonshire theory, independent of the poling direction and domain configuration. For example, single crystal $Pb(Mg_{1/3}Nb_{2/3})O_3$-$PbTiO_3$ is calculated to have g_{33} values of 38.9, 40.1, and 33.5×10^{-3} Vm/N when poled along the pseudo-cubic [001], [011], and [111], respectively [7]. Rhombohedral $Pb(Yb_{1/2}Nb_{1/2})O_3$-$PbTiO_3$ [19] poled along the pseudo-cubic [001] show a useful g_{33} of 64.6×10^{-3} Vm/N, however, this is still significantly below values for orthorhombic and tetragonal systems. Like orthorhombic systems, the lack of crystallographic data and wide degree of processing variability results in difficulties when providing a mechanistic outlook on these systems, however they are unlikely to promote significant technological leaps in applications that require high g_{ij} coefficients.

2.1 Materials and Limitations

Significantly large g_{ij} values have been reported in and calculated from literature for $PbTiO_3$ [20-22], $BiScO_3$-$PbTiO_3$ [23, 24], $Bi(Zn,Nb)O_3$-$PbTiO_3$, and $Bi(Zn,Ti)O_3$-$PbTiO_3$ [25] single crystals. The trend in Figure 2 also raises the notion of single crystal $BiFeO_3$-$PbTiO_3$ potentially possessing significantly large g_{ij} coefficients owing to its large tetragonality [26-30]. Although tetragonal $BiFeO_3$-$PbTiO_3$ single crystals have successfully been grown [31, 32], no piezoelectric properties have been measured to date. However the practical limitations associated with fabrication of tetragonal single crystals are severe and scalability remains questionable. Although the flux growth of single crystals is a common method and is responsible for most experimental datapoints in this section, sample size is often limited to 1-10mm due

to slow growth rates associated with this technique. Arguably the most scalable method of growing ferroelectric single crystals is by the modified Bridgman method where single crystals of PMN-PT on the scale of 3 inch diameter have been achieved and are commercially available [33]. This method is well suited for growing rhombohedral crystals where the volume expansion when cooling through the Curie temperature is <1% and thus the only limitations are the size of furnace and crucible. However for tetragonal crystals, the physical constraints of the platinum crucible wall and the volume expansion of the material when cooling through T_C results in intense cracking or even complete disintegration of samples. Sufficiently large orthorhombic $(K,Na)NbO_3$ single crystals have also been grown by the modified Bridgman method [34, 35] which when combined with the ability to exhibit large g_{ij} coefficients, makes them promising candidates for the future.

Commercial barium titanate with a tetragonality of approximately 1.1% is processed using top seeded solution growth (TSSG) which overcomes the issue of crucible constraints [36-38]. However the open crucible set-up that is adopted for TSSG combined with the volatility of bismuth and lead oxides results in exposure time limitations and subsequently limited crystal size and/or deviation from desired stoichiometry. Liu et al. [25] found when growing $Bi(Zn,Ti)O_3$-$PbTiO_3$ and $Bi(Zn,Nb)O_3$-$PbTiO_3$ crystals that although the nominal stoichiometry was calculated to be $0.40Bi(Zn,Ti)O_3$-$0.60PbTiO_3$ and $0.30Bi(Zn,Nb)O_3$-$0.70PbTiO_3$, energy dispersive x-ray analysis indicated stoichiometry of the as-grown crystals to be $0.14Bi(Zn,Ti)O_3$-$0.86PbTiO_3$ and $0.38Bi(Zn,Nb)O_3$-$0.62PbTiO_3$.

3 Polycrystalline Ceramics

Polycrystalline ceramics offer a low-cost, high-throughput alternative compared to single crystal and textured ceramics and therefore dominate the scope of materials research publications. As shown in Figure 1, g_{33} values of commercially available materials are relatively unspectacular. Despite this, modified PZT polycrystalline ceramics are typically used in sonar transducers with the two common Navy-type piezoceramics employed being Navy-type I and II, both of which are used in passive devices. In an industrial setting, Navy-type piezoceramics may also be referred to by their commercial product code with the PZT400 and PZT500 series representing Navy-type I and II, respectively. However in academic environments, Navy-type I is more commonly referred to as 'hard' or acceptor-doped PZT and Navy-type II as 'soft' or donor-doped PZT. The capacity to withstand depoling when exposed to elevated drive conditions or mechanical stress leads to the preferred use of Type I (hard PZT) within devices experiencing high hydrostatic pressures at significant marine depths. Navy-type I compositions also exhibit lower values for g_{31} compared to Type II (soft PZT) which subsequently increases g_h and hence the open circuit receive sensitivity of an unbaffled hydrophone operating under free field conditions. Modified $PbTiO_3$ polycrystalline ceramics have also been a favoured choice for hydrophone applications

with mentions of its popularity going back to the 1980s [39]. Its usefulness stems from significant intrinsic decoupling between 33 and 31 modes resulting in desirable hydrostatic properties compared to $Pb(Zr,Ti)O_3$ [40-46].
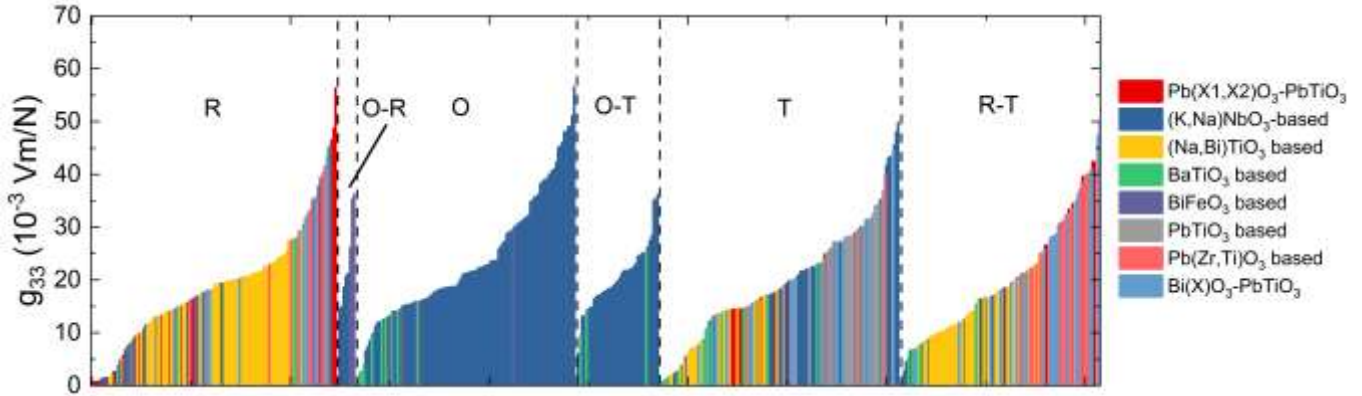

Figure 5: Piezoelectric g_{33} coefficients for a range of polycrystalline ceramic materials categorised by crystallographic phases and by base material. R - rhombohedral, O - orthorhombic, T tetragonal. Material property data can be found in supplementary material.

Finding alternative materials with enhanced piezoelectric voltage coefficients compared to modified PZT and $PbTiO_3$ in polycrystalline form provides the opportunity for applications where low-cost, high throughput processing is desirable such as monolithic hydrophones. Figure 5 shows g_{33} values in ascending order for a range of polycrystalline materials possessing tetragonal, orthorhombic, rhombohedral and mixed crystallographic phase (material property data found in supplementary data). Despite providing a low-cost fabrication route, bulk polycrystalline ceramics exhibit unremarkable piezoelectric voltage coefficients independent of structural phase, with largest values being 49.7×10^{-3} Vm/N (0.95KNN-0.05LN [47]), 56.5×10^{-3} Vm/N (KNN [48]), and 56.3×10^{-3} Vm/N (0.1PMN-0.1PFN-0.8PZT [49]) for tetragonal, orthorhombic and rhombohedral systems, respectively. Although some doped $BiFeO_3$ rhombohedral polycrystalline materials demonstrate high g_{33} values $<92 \times 10^{-3}$ Vm/N [50], these values are more likely the result of the unintended but significant effect of porosity and therefore is a reflection of microstructural effects as oppose to a reflection of the chemistry or physics.
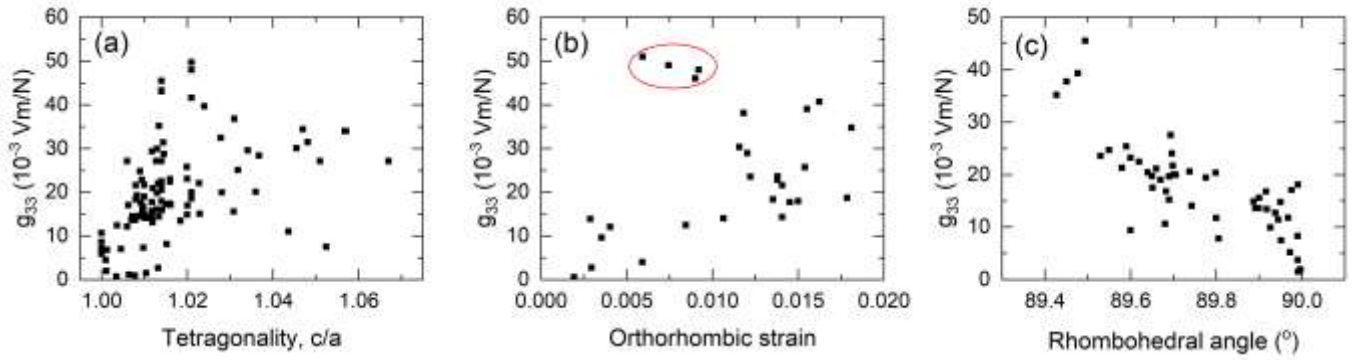
Figure 6: Piezoelectric g_{33} coefficient as a function of crystallographic strain in the (a) tetragonal, (b) primitive orthorhombic, and (c) rhombohedral phases. Tetragonal strain is defined as the ratio between the c and a lattice parameters, orthorhombic strain is defined as the difference between the maximum and minimum lattice parameter relative the equivalent cubic setting as in Ref. [51], and rhombohedral strain is defined as rhombohedral tilt angle which correlates to the c/a ratio when in the hexagonal context. Outlined datapoints in (b) are highlighted to show potential deviation from trend.

It is most likely that the more complex microstructure in polycrystals and the subsequent intergranular effects have drastic effects on electrical properties similar to behaviour observed for the piezoelectric d_{ij} coefficient. The significant difference between polycrystals and single crystals is microstructure, with polycrystalline samples made up of many grains which lack any long-range orientation, whilst single crystals consist of one grain with long range translational symmetry, the effects of which are discussed in further detail later in this section. Furthermore, contrary to single crystal and textured ceramics where the crystallographic dependence of the piezovoltage coefficient is recognisable, for polycrystalline ceramics, the inherent contribution from the crystallographic phase is dwarfed by processing and chemical contributions such as poling efficiency, grain size and distribution, doping regime, and as will be discussed in Section 5, the significant effect of porosity. Despite the wide range of g_{33} values, $(K,Na)NbO_3$-based materials show the highest values in both the orthorhombic and tetragonal setting [53,54]. The role of electronegativity in these systems has been a proposed mechanism [52], however this relationship has been found to be unclear when considering a wider range of materials [53].

Figure 6 shows g_{33} values for polycrystalline materials as a function of their crystallographic strain. Whilst for single crystals the tetragonality appears to be the primary driving force (Figure 2), for polycrystalline samples the relationship is more complicated. A wide distribution for g_{33} can be observed which is attributed to the much wider variation of significant parameters compared to single crystals as mentioned earlier, with peak values achieved between 1.015 and 1.025 tetragonality. The initial increase in g_{33} may be attributed to the increasing polarisation concordant with behaviour for single crystals,

however above 2.5% tetragonality the g_{33} continuously decreases. Leist et al. [54] used the case study of La-doped $BiFeO_3$-$PbTiO_3$ polycrystalline ceramics to study the effect of tetragonal strain on the piezoelectric and dielectric properties. It is found that above a critical tetragonality of 1.045 the suppression of domain switching resulted in d_{33} values of 10-20pC/N, whereas below the critical tetragonality d_{33} values of up to 10 times greater are measured. It is also postulated that the nucleation of new domains through the application of an external electric field is energetically unfavourable due to the enormous elastic energy for highly tetragonal materials. Li et al. [55] showed an increase in domain wall density with increasing La content for La-doped BF-PT. Although not explicitly stated by the author that this was a result of decreasing domain wall strain energy through decreasing tetragonality, it may be a likely cause. Yoon et al. [56] have also investigated the influence of tetragonal strain on piezoelectric properties of (1-x)$BaTiO_3$-(x)$Bi_{0.5}Na_{0.5}TiO_3$ polycrystalline ceramics. It was found through transmission electron microscopy and polarisation-electric field loops that an increase in tetragonality reduces reversible domain wall contributions to piezoelectricity and reduces irreversible domain wall mobility. Furthermore, high-energy X-ray diffraction studies have also shown a decrease in 90° domain wall motion at increasing tetragonalities [57]. As domain wall density and motion heavily influence the piezoelectric properties, the suppression of domain walls though intergranular stress leads to low d_{33} and therefore low g_{33} values in polycrystalline samples.

For orthorhombic systems, the increased number of potential crystallographic contexts dilutes datapoints creating difficulties in establishing structure-property relations. When g_{33} is plotted as a function of crystallographic strain in the primitive orthorhombic context, two potential trends occur depending on the validity of datapoints circled in Figure 6 (b). Firstly, a similar trend to tetragonal materials could occur in which there is an initial increase <0.075 at which point the g_{33} decreases due to intergranular stresses and subsequent suppression of domain wall motion and nucleation. Alternatively, it is possible that the highlighted datapoints from Ref. [58] are subject to relatively high, unintended porosity, enhancing the g_{ij} and providing ambiguity to the trend in which case a positive correlation between strain and g_{33} is observed. In the former, the microstructural effects which suppress the g_{33} occur at significantly smaller strains compared to tetragonal materials therefore making the latter more likely. However, it must be noted that similar plots in the pseudo-monoclinic and pure orthorhombic phase (Figure S2) show no observable correlations.

Figure 6 (c) shows that for rhombohedral materials, a correlation between rhombohedral angle which is coupled to polarisation and g_{33} is observed. Unlike tetragonal materials, rhombohedral materials do not show a suppression of g_{33} owing to the relatively subtle crystallographic strains and therefore the limit to a tolerance-based design approach is unclear. However it is likely that further enhancement of

tilting will either result in a polymorphic phase transition or increase perovskite instability and encourage the formation of undesirable, non-piezoelectric phases.

Overall, despite polycrystalline ceramics possessing significantly lower piezoelectric voltage coefficients compared to single crystals, textured ceramics, and composite materials, the usefully large g_{33} of some materials, namely KNN-based, compared to commercially available PZT and modified $PbTiO_3$ ceramics results in the emergence of promising candidates for low-cost applications such as monolithic hydrophones. However it must be considered that the popularity of modified $PbTiO_3$ is due to the significant 33-31 mode decoupling resulting in high g_{33}/g_{31} ratios and impressive hydrostatic properties. Therefore, from a materials science perspective, obtaining the full piezoelectric property matrices are an important step for any promising candidates in order to assess hydrostatic properties. Further considerations, particularly from an industrial perspective, must also be made as discussed in Section 7 before these can be transitioned into industry.

4   Textured Ceramics

Textured ceramics provide an intermediate between single crystals and polycrystalline ceramics. Although the presence of grains and grain boundaries is similar to polycrystalline ceramics, the microstructure is designed to provide a degree of crystallographic and polarisation alignment similar to single crystals. The texturing of ceramics to enhance g_{ij} is a relatively new research area, however has thus far been successfully demonstrated with $0.99(K_{0.49}Na_{0.49}Li_{0.02})(Nb_{0.97-x}Sb_{0.03}Ta_x)O_3$-$0.01CaZrO_3$ [59] and $(Ba,Ca)(Ti,Zr)O_3$ [60] showing an 85% and 174% increase in g_{33} compared to non-textured ceramics.

However these values remain relatively low achieving 30.3×10^{-3} Vm/N and 34.3×10^{-3} Vm/N, respectively. The most significant g_{33} has been measured by Yan et al. [61] where Sm and Mn co-doped $PbTiO_3$ textured ceramics were fabricated using templated grain growth method. As the degree of texturing increases, the piezoelectric d_{33} increases from 53pC/N for non-textured ceramics to 95pC/N and 127pC/N for 82% textured and 95% textured, respectively. The relative permittivity decreases with increasing texture giving values of 202 for non-textured, 146 for 85% textured and 124 for 95% textured samples. Reasons for the enhancement of the d_{33} and suppression of the dielectric permittivity are analogous with those of single crystals. As the texturing degree increases, the angle between crystallite polarisations and the polar axis, where a maximum d_{33} for an extender ferroelectric and a minimum relative permittivity is observed, decreases. The simultaneous increase in d_{33} and decrease in the permittivity results in g_{33} increasing from 30×10^{-3} Vm/N for polycrystalline $PbTiO_3$ to 74×10^{-3} Vm/N for 82% textured ceramics and 115×10^{-3} Vm/N for 95% textured samples.

Unlike single crystal systems, the crystallographic dependence of g_{33} for textured ceramics is more in line with Landau-Devonshire theory where the highest reported values for rhombohedral systems (53.8×10^{-3} Vm/N [62]) are relatively low, followed by orthorhombic systems (82.5×10^{-3} Vm/N [63]) and finally tetragonal systems exhibiting the highest reported value for g_{33} (115×10^{-3} Vm/N [61]). However more datapoints are needed to provide a general view of crystallographic dependence.

5   Piezoelectric Composites

In this section, both ceramic-matrix and polymer-matrix composites and their effective properties are discussed. In the former, a bulk piezoelectric ceramic with high piezoelectric charge coefficient and relative permittivity is replaced with a low permittivity second phase (e.g. air/polymers) to decouple the piezoelectric and dielectric properties. In this case, the aim is to significantly reduce the permittivity whilst maintaining high piezoelectric properties; the largest decoupling of these properties is typically observed in soft ferroelectrics that usually have a large permittivity. The latter involves the introduction of a piezoelectrically active phase to a polymer, with the main aim being to achieve relatively high d_{33} values through microstructural design. For the purposes of this review, porous ferroelectric ceramics will be considered as ceramic-matrix composite systems, as porosity plays a key role in engineering the functional properties of the material.

It is useful to consider the microstructural connectivity of a piezoelectric composite before understanding the mechanisms behind the enhanced voltage coefficient. Newnham et al. [64] first proposed the 'X-Y' notation where X and Y represent the self-connectivity of the ceramic and secondary phase, respectively. Shown in Figure 7, a piezoelectric composite formed of an isolated piezoelectric phase in an inactive polymer matrix has a 0-3 connectivity, a laminated piezoelectric-polymer composite has 2-2 structure, and a porous ceramic with interconnected porosity has a 3-3 structure. The connectivity and resultant properties of a two- or more-phase material are closely linked to the processing method.
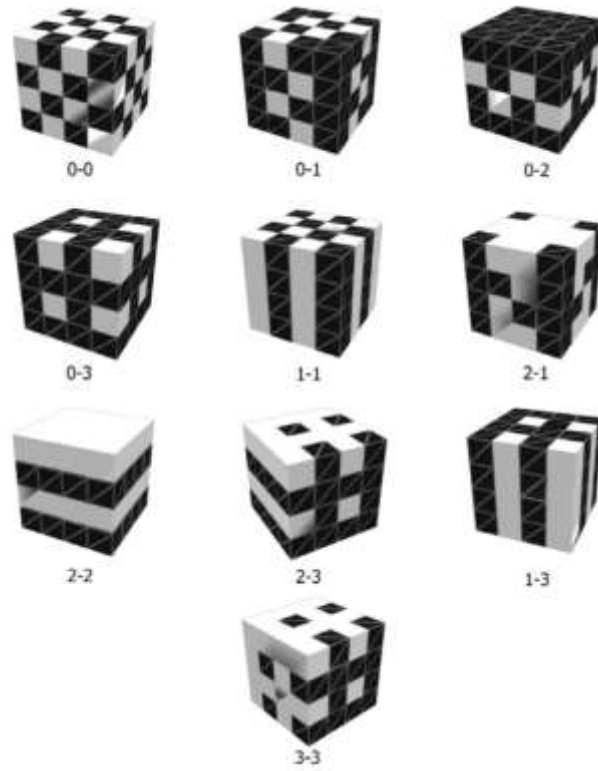
Figure 7: Connectivity families for diphasic composites. Taken from [65] with permission through IEEE (License number: 4941430127676)

5.1 Ceramic-Matrix Composites

The introduction of low permittivity and low stiffness second phases such as pores or polymer/elastomers into a bulk ferroelectric ceramic has multiple benefits. Firstly the reduction of ferroelectric volume fraction leads to a significant dilution of the relative permittivity and a reduction in the d_{33} of the composite. However an increase in g_{33} can be achieved if the rate of decrease of the relative permittivity exceeds the rate of decrease of the d_{33} [66, 67]. Due to the infinite compliance of pores, all applied mechanical force goes through the ferroelectric phase in a porous ceramic which increases local stress concentrations and yields relatively large d_{33} values. As the volume of high permittivity material is reduced, the ability for the material to polarise in the opposite direction to the generated piezoelectric voltage through local movement of ions or ferroelectric domains decreases. This leads to a higher output voltage for a given applied stress and therefore a high g_{ij} coefficient. Introducing a polymer with a finite compliance results in a proportion of the load transferring through the passive phase causing the effective d_{33} to decrease faster than for porous ceramics of the same ceramic volume fraction [68]. Therefore, selecting a polymer with a lower stiffness such as polyurethane foam is

favourable compared to using higher stiffness epoxy as the second phase for achieving a high g_{ij} coefficient [69].

Furthermore the introduction of a low stiffness second phase leads to a decoupling between the longitudinal (33) and transverse (31) modes. When a force is applied transverse to the poling direction in a piezoelectric composite, the efficiency of transferred load into the 3-direction is reduced [70]. As the volume fraction of the low permittivity second phase is increases beyond ≈0.5, the d_{31} (and g_{31}) tends to zero whilst still exhibiting a relatively large d_{33} coefficient [66]. This phenomenon results in enhanced hydrostatic charge coefficient compared to dense polycrystalline and single crystal ceramics, where the crystallographic symmetry results in $|d_{31}| \approx 0.5d_{33}$ and thus limits d_h. As the hydrostatic charge coefficient is increased and the relative permittivity reduces, large improvements in the hydrostatic voltage coefficient g_h can be realised [71, 72].

In ceramic-matrix piezoelectric composites, porosity can be introduced intentionally during processing of the bulk ceramic using methods such as coral replica method, burned-out polymer spheres (BURPS) method, direct foaming, gel- or freeze-casting, direct write, or 3D printing [66, 73-75]. In the BURPS process, a volatile organic pore former is mixed with the ceramic powder before pressing. During sintering, the organic burns out leaving voids in the material that have a material that have a similar morphology to the pore former [72]. Direct foaming introduces gas into a slurry, which is stabilised before drying and sintering, and gel- and freeze-casting are also formed from a liquid phase with porosity introduced into the system through direct solidification of a second phase that is then removed during or prior to sintering. Freeze-casting has been shown to be an effective method of producing highly aligned porous structures through directional freezing of a solvent, usually camphene or water, prior to sublimation of the solvent and sintering of the ice-templated structure. The structures can then be filled with a polymer second phase after sintering. Printing ceramic structures has also gained interest in recent years [75], and excellent effective properties can be achieved by forming meta-structures that manipulate local electric and mechanical fields to promote high g_{33} and g_h coefficients [76, 77].

The methods of directly introducing porosity into the ceramic before or during sintering have an advantage over top-down approaches whereby a dense, sintered block is machined to leave the desired composite structure. The dice-and-fill method is commonly used to produce 1-3 composites (more details in Section 5.2), and early research in this field also investigated perforated piezoelectric composites, whereby holes are drilled in poled, dense ceramic. This method was successful in reducing the permittivity of the material whilst maintaining a relatively high charge coefficient leading to an improvement g_{33} [78]. However, these processes are relatively inefficient as high volumes of sintered material must be machined away and are either lost or need to be recycled, adding cost to the process compared to fabricating a near-net shape porous structure.

As with all ferroelectrics, poling is required after sintering to induce piezoelectric properties. This is complicated by the presence of high volumes of pores, as the electric field preferentially concentrates in the low permittivity phase resulting in incomplete poling of the ferroelectric and a decrease in d_{33} and therefore g_{33} [79, 80]. Techniques such as freeze-casting, where the porous structure can align to the poling direction, results in a more homogeneous local electric field during poling and high d_{33} coefficients, however the permittivity tends to be higher than for materials with randomly distributed porosity (see Table 1) [81]. An exception to this rule was observed in porous barium titanate fabricated by freeze casting with anisometric pores aligned to the poling direction had a lower permittivity compared to barium titanate with randomly distributed pores fabricated by the BURPS method [82]. This behaviour has been attributed to dielectric anisotropy in the $P4mm$ crystal structure where $\varepsilon_{11} \gg \varepsilon_{33}$, and a degree of texturing introduced through the freeze-casting procedure. A combination of microstructural texturing and utilising a low permittivity second phase such as porosity, could be a potential method for further improving the voltage sensitivity of piezoelectric composites, a principle that has been demonstrated previously [83].

The first study utilising piezoelectric composites to achieve high g_{ij} coefficient was reported by Skinner et al. [64] whereby PZT/polymer composites were formed by infiltrating a porous PZT framework with an elastomer. A porous PZT structure was formed by the coral replamine procedure in which a wax negative was made from calcium carbonate into which PZT was slip-cast. The negative was burned off during sintering leaving a consolidated porous PZT structure and a passive second phase was added prior to poling. This processing resulted in a significant increase in g_{33} from 20×10^{-3} Vm/N for dense PZT-501A to 282×10^{-3} Vm/N for a PZT volume fraction, $v_f = 0.35$. Although this composite had 3-3 connectivity by design, the material was strained to the extent that the ceramic fractured within the polymer, leaving isolated regions of PZT to form a 0-3 structure which further increased the maximum g_{33}. Lee et al. [84] have reported the largest g_{ij} values to date for porous ferroelectric ceramic composites for freeze-cast PZT-lead zinc niobite (PZN) with an active volume fraction, $v_f = 0.1$, and pores aligned to the poling axis. These structures resulted in a g_{33} and g_h of 442×10^{-3} Vm/N and 360×10^{-3} Vm/N, respectively. At volume fraction, $v_f = 0.66$, the highest piezoelectric voltage coefficient was found when highly anisometric pores were orientated perpendicular to the poling direction, with $g_{33} = 216 \times 10^{-3}$ Vm/N, compared to 41×10^{-3} Vm/N when pores were orientated to the poling direction [85]. Reducing the v_f of the active phase further whilst aligning pores perpendicular to the poling direction may further increase g_{33} and g_h. In general, the most successful studies have utilised a soft PZT system in which poling is significantly easier compared to ferroelectrically harder systems. Table 1 shows the highest g_{33} and g_h values for different processing methods and microstructural connectivity.

Table 1: Piezoelectric voltage coefficients for a variety of ceramic-matrix composite constituent materials, composite structures and volume fractions from literature

Material (active:passive)	Composite structure	Process	Volume fraction (active phase)	g_{33} (10^{-3} Vm/N)	g_{31} (10^{-3} Vm/N)	g_h (10^{-3} Vm/N)	Ref.
PZT-PZN:Air	3-3 aligned	Freeze-casting (camphene)	0.1	442.0	-41.2	359.5	[84]
PZT-PZN:Air	3-3 perpendicular	Freeze-casting (camphene)	0.1	341.1	-24.8	291.4	[84]
PZT501A:Polyurethane foam	1-3 aligned	Arrange and fill	0.04	320.9	-5.1	310.6	[69]
PZT501A:Silicone elastomer	0-3	Coral replamine	0.35	282.4			[86]
Nb-PZT:Air	3-3	BURPS (MHEC)	0.62	223.2	-40.9	141.3	[71]
PZT NCE-55:Air	3-1 perpendicular	Freeze-casting (water)	0.63	215.7			[85]
PZT NCE-55:Air	3-1 aligned	Freeze-casting (water)	0.63	41.9			[85]
PZT501A: Silicone elastomer	3-3	BURPS (PMMA)	0.3	211.8	-86.1	39.5	[87]
PZT501A:Epoxy	3-3	BURPS (PMMA)	0.3	67.3	-5.2	56.3	[87]
PZT5H:Air	3-3	BURPS (PMMA)	0.365	186.6	-3.0	180.6	[72]
PZT5H: Air	3-3	Coral replamine	0.073	183.3	-1.1	193.9	[72]
PZT-PZN: Air	3-1 aligned	Freeze-casting (camphene)	0.18	149.3	-17.2	114.9	[88]
PZT501A:Epoxy	1-3 aligned	Arrange and fill	0.1	135.5	-45.7	44.0	[89]
PZT501A:Epoxy	3-2 perpendicular	Cross-perforated		112.9	7.6	128.1	[78]
PZT501A:Epoxy	3-1 perpendicular	Cross-perforated		72.8	-8.5	55.7	[78]
PZT501 Zibo:Air	3-1 aligned	Freeze-casting (water)	0.4	71.4	-14.4	42.6	[90]
PZT501 Zibo:Air	3-3	Freeze-casting (water)	0.4	154.3	-60.6	33.1	[90]

Whilst forming ferroelectric composites is an effective method of increasing g_{33} and g_h values beyond those that can be readily achieved in polycrystalline ferroelectric systems, it should be noted that often a high permittivity is required to overcome inherent capacitances in external electronics that convert piezoelectric signals into useful information. This is true for medical imaging devices, where a reduction in the permittivity and therefore the capacitance of the active material can reduce the spatial resolution of the imaging device [91], and also for sonar devices where low piezoelectric material capacitance can reduce the signal-to-noise ratio and subsequently the sensitivity of a device [92].

5.2   Polymer-Matrix Composites

As mentioned previously, polymer-matrix composites involve the introduction of a piezoelectric ceramic into a polymer with the aim of increasing piezoelectric activity of the system. Although ferroelectric polymers have relatively low dielectric and piezoelectric properties compared to bulk systems and ceramic-matrix composites, they possess low acoustic impedance, are flexible, ductile and can be manufactured with various processing techniques. The PVDF family is the most well-studied and commercially available ferroelectric polymer system with nylon and PVC having also been reported [93-96] achieving g_{33} values between 150-600x10^{-3} Vm/N. Due to the high coercive field and the need for mechanical poling of PVDF polymers, researchers in the 1970s started exploring piezoelectric composites by incorporating an active piezoelectric ceramic filler in a passive polymer matrix. Kitayama and Sugawara [97] first published work on hot-rolled PZT-PVDF composite reporting a significant improvement in piezoelectric properties with respect to PVDF, whilst still retaining mechanical flexibility.

The first generation of polymer-matrix composites displayed 0-3 configuration [98-104] with significantly lower piezoelectric properties compared to ceramics as a result of insufficient poling of ceramic particles at low volume fractions. Due to the lower permittivity of the polymer phase, the electric flux concentrates more effectively on the polymer phase and does not affect the ceramic particles efficiently. Changing the morphology of the ceramic filler to a fibrous distribution (1-3) with continuous ceramic fibres fully aligned in one-dimension results in an increase in the piezoelectric charge coefficient up to the value of the constituent ceramic [105]. Two strategies for forming 1-3 piezoelectric composites are the dice-and-fill and arrange-and-fill methods [89, 106]. In the dice-and-fill method, a dense ceramic either single crystal or polycrystalline is machined to form highly aligned 1-3 type structures that are then filled with a polymeric second phase. The arrange-and-fill method uses extruded and sintered piezoelectric ceramic fibres arranged into a 1-3 pattern before curing in a polymer.

Composites with 0-3 and 1-3 type connectivity represent the lower and upper bounds as far as the piezoelectric charge coefficients are concerned. An intermediate state between 0-3 and 1-3 state can be obtained by applying a dielectrophoresis (DEP) structuring treatment on a ceramic particle and

uncured polymer matrix [107, 108], where the piezoelectric ceramic particles align in chain-like structures parallel to the applied field. These systems can exhibit large g_{33} values at low filler volume fractions while maintaining high mechanical flexibility [109-116]. The peak in performance has been attributed to the higher poling efficiency, hence the significantly higher d_{33} in DEP composites, whilst the relative permittivity is dominated by the polymer and is nearly independent of microstructural connectivity [117, 118]. The increased poling efficiency in these composites compared to 0-3 composites is due to the very low interparticle distance ($<2\mu$m) within chains spanning two electrodes, resulting in continuous percolating paths. Such a lower polymer layer thickness facilitates the poling of the composite, as a smaller fraction of the applied external electric field is imposed on the polymer matrix rather than on the poling of the ceramic particles.

The number of particle interconnections within a DEP chain can be minimised using high aspect ratio fibres instead of equiaxed particles. High aspect ratio fibres also enhance the DEP structuring efficiency and result in a shift of the maximum g_{33} to lower filler volume fractions [119, 120]. The largest piezoelectric voltage coefficient reported to date for ferroelectric ceramic-polymer composite is 510×10^{-3} Vm/N for potassium sodium lithium niobate (KNLN) ceramic fibres of volume fraction, $v_f = 0.06$, dielectrophoretically structured in a flexible polydimethylsiloxane (PDMS) matrix [120]. At higher filler volume fractions, the d_{33} of the composites increases at a slower rate than the permittivity, which increases approximately linearly with ceramic volume fraction and therefore the overall g_{33} decreases.

6 Applications

The piezoelectric voltage coefficient presents a proportionality coefficient that is the figure of merit in many applications and therefore striving to achieve a high g_{ij} is the primary driving force in designing new materials. Examples include hydrophones in defence and fishing sectors, accelerometers and engine knock sensors in automobiles and aeronautics, and e-skins in robotics [3, 65, 92, 121-124]. To observe how g_{ij} relates to performance in these applications, it is useful to derive the relationship with voltage. As external stimuli induce stresses within the piezoelectric material to generate an electric field, E, the behaviour can be described by the constitutive equation of piezoelectricity shown in Equation 11.

$$E = -gX + \beta^T D \tag{11}$$

Where g is the piezoelectric voltage coefficient, X is stress, β^T is the impermittivity at constant tensile stress and D is the electric displacement. When a piezoelectric material is poled perpendicular to the electrodes the component of the electric field along the 3-direction, E_3, can be defined as:

$$E = -g_{31}X_1 - g_{32}X_2 - g_{33}X_3 + \beta^T_{33}D_3 \tag{12}$$

The voltage generated between the two electrodes is defined using Equation 13.

$$V = \int_{-\frac{t}{2}}^{\frac{t}{2}} E_3 dz = E_3 t \tag{13}$$

Where z is the polar direction and t is sample thickness. Combining Equations 12 and 13 for an open circuit condition ($D=0$) gives:

$$V = -g_{31}tX_1 - g_{32}tX_2 - g_{33}tX_3 \tag{14}$$

6.1   Polymer-Matrix Sensors

As mentioned in section 5.2, polymer-matrix composites show superior g_{ij} coefficients due to their low permittivity. However it is their other advantages such as high compliance, which leads to good impedance matching with the human body, and a low mechanical quality factor allowing for broad resonance band width, which make these materials suitable for large area and flexible sensing applications such as robotic skins [115, 122, 125-127], tactile imaging [128], and wearable strain sensors [123].

Recent advancements in autonomous intelligent robotics has encouraged the development of humanlike skin with multi-sensory tactile capabilities as covered by several comprehensive review papers [123, 125, 129, 130]. These robots with enhanced human-machine functionalities can have an extended range of applications in and exploratory areas [130]. The most primary function of skin, the sense of touch to perceive contact, is integrated using piezoelectric sensor arrays [126, 127, 131, 132]. The need to mimic the mechanical properties of human skin, in particular the flexibility, to accommodate various motions is the second key function that highlights the importance of the choice of the sensing material to achieve desired functional and mechanical properties [121, 133].

6.2   Energy Harvesting

Over the past two decades there has been a rapidly growing interest in the use of piezoelectrics to harvest mechanical energy from ambient vibrations and convert it into usable electrical power [134]. The implementation of self-powered sensor networks would remove the requirement for wiring sensors to the mains power, allowing them to be used in difficult-to-access areas such as boreholes for oil and gas and inside automotive tyres for pressure monitoring [135]. The scavenged energy can also be used to recharge batteries, reducing the number of costly maintenance events for battery replacement and avoiding the environmental impact associated with battery disposal. Whilst energy harvesting from ambient sources of energy and the by-products of thermodynamic processes is not going to generate

on a scale required for lighting and heating buildings (typical output power range has been stated in the order of μW to mW [136]), benefits lie in relatively small improvements in efficiency (e.g. in transport and energy generation), reduced maintenance and increased longevity of devices.

Whereas the sensitivity of piezoelectric sensors is dependent on generating a voltage in response to a mechanical excitation such that a large g_{ij} coefficient is favourable, piezoelectric energy harvesters require the output power to be maximised. The most commonly used figure of merit is therefore $d_{ij}.g_{ij}$ [137] for off-resonance, or broadband, harvesting. Whilst a high g_{ij} is important, a high d_{ij} coefficient is simultaneously required, and in dense ferroelectrics a high charge coefficient can dominate this term. Therefore soft PZT is much more commonly used than hard PZTs for this application. Porosity and the forming of ferroelectric composites can also improve output power for a given input mechanical stress, however the need for high d_{ij} coefficients mean that microstructural alignment can be more important for sensing applications, hence the interest in freeze cast materials for harvesting applications [138] . Matching the mechanical and electrical impedance of the active piezoelectric element to improve energy transfer also needs to be considered, and composites can be used to alter the mechanical and electrical properties of the material whilst still achieving high d_{ij} coefficients as discussed previously in Section 5.1. However the decrease in the transverse piezoelectric coefficient seen in composites can be detrimental to harvesters that are often designed to operate in bending mode [138], and as such careful design of microstructure is required to ensure adequate transfer of stress into the polarisation axis. Macro-fibre composites (MFCs) achieve this by aligning fibres to the mechanical stress direction, poling through thickness and using interdigitated electrodes [139]. Energy harvesting and sensing from pressure waves in hydraulic systems have also been studied recently [140], requiring materials with high hydrostatic responses. The application of ferroelectric materials for sensing and energy harvesting, and indeed electrical energy storage in the form of capacitors, provides the unique potential to create self-powered intelligent sensing devices in the near future, although the subtlety different material requirements of the sensing, harvesting and storage mechanisms require careful consideration and design.

6.3   Sonar Applications

Sonar (sound navigation ranging) systems use the propagation of sound waves to communicate with, or to detect, classify, and locate objects which are located on the surface or beneath a body of water. Sonar systems operate under two fundamental conditions, active and passive, and although different transduction mechanisms such as magnetostrictive [141, 142] or optical [143-145] systems are available, piezoelectric transduction is used in most sonar systems.

Active sonar systems generate an acoustic signal using a projector, which propagates through the water to an object of interest where it is 'insonified' and an acoustic signal is returned as an echo. By

using the time between transmission of the acoustic signal and the return of the echo, the speed of sound of water, and the direction from which the echo is returned, the baring, range, and quite often classification of the object can be calculated.

Passive sonar systems employ hydrophones which are only designed to detect (or receive) self-generated acoustic signatures radiating from an object of interest. These signatures can stem from rotating components on ships, such as pumps or propeller shafts, or have a biological source such as from fish or marine mammals. A basic passive sonar system, consisting of a single or a limited number of hydrophones may only be able to provide very basic information such as the existence of an object. However more complex hydrophone arrays can provide additional information such as the range, baring, and classification of an object. Piezoelectric voltage coefficients are important considerations when designing hydrophones for passive sonar systems. To demonstrate the influence that it can have on the sensitivity of a hydrophone, the set-up involving a plate of piezoelectric material operating under free-field conditions and below resonance as shown in Figure 8 will be considered. The response of more complex configurations are considered and readily available in literature [92, 124]. Hydrophones generate an output voltage which is proportionate to the amplitude of the incident pressure wave contacting the surface of the hydrophone, the ratio of which represents the hydrophone sensitivity, M.

$$M = \frac{V}{p_i} \tag{15}$$

Where V is voltage from Equation 14 and p_i is incident wave pressure. For free-field conditions (Figure 8 (a)), the pressure, and hence stress exposed across the surface of the hydrophone are equal, $X_1 = X_2 = X_3$. Combining Equations 14 and 15, provides the free-field receive sensitivity under hydrostatic conditions, M_h:

$$M_h = g_{33}t + g_{32}t + g_{31}t = g_h t \tag{16}$$

If the unelectroded sides of the hydrophone are baffled as depicted in Figure 8 (b), the stress conditions in these directions reduce to zero, $X_1 = X_2 = 0$. As the electroded surface is still exposed to the incident wave, X_3 is non-zero and is equal to p_i. Incorporating these stress conditions gives the 33-mode hydrophone sensitivity, M_{33}.
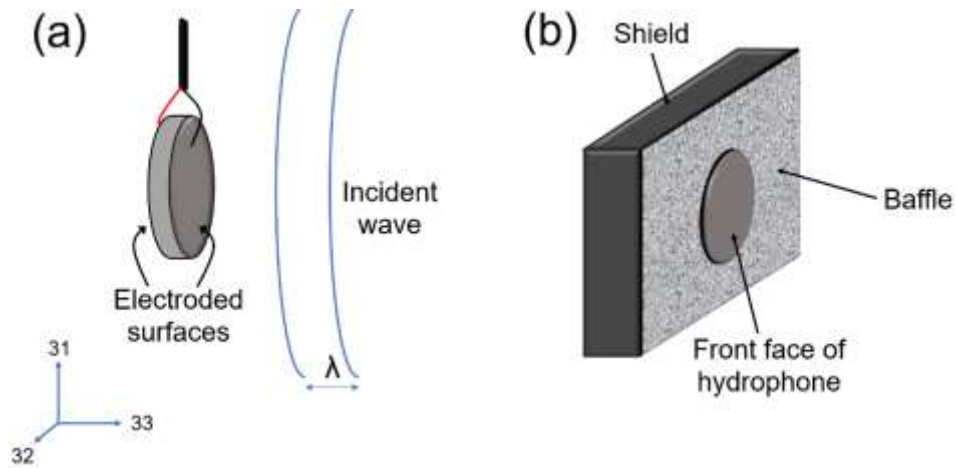
$$M_{33} = g_{33}t \tag{17}$$

Figure 8: Schematic of a (a) baffled, and (b) unbaffled hydrophone in 33-mode

7 Integration of new high g_{ij} piezoelectric materials into industry: A sonar perspective

As mentioned previously, modified PZT and $PbTiO_3$ polycrystalline ceramics are typically used in sonar transducers and due to the wide range of modified PZT compositions available, the US military standard, MIL-STD-1376B [146], provides a useful tool to compare compositions against different operating scenarios. For the sake of this section, 'new' piezoelectric materials define materials that fall outside of the scope of mainstream commercial piezoelectrics such as polycrystalline PZT and $PbTiO_3$, indiscriminate of chemical composition or material form.

As previously discussed in Section 5, piezoelectric voltage coefficients of Navy-type I (hard) and II (soft) PZT compositions can be enhanced through manufacturing piezo-composite transducers [147]. This enhancement in performance is often utilised in sonar systems which are required to generate high resolution images, such as multi-beam echosounders and side scan sonar which can be used to map the sea floor. However not all sonar systems require such performance and so the relative high cost of composites, when compared to monolithic elements of piezoelectric material, can cause them to be uneconomical. Modified $PbTiO_3$ polycrystalline ceramics possesses a usefully high g_h, when considering the modest values it exhibits for g_{33} and d_{33}, due to their low piezoelectric response (d_{31} and g_{31}) in the lateral directions [40-46]. As it is typically employed within a sonar transducer as a monolithic element, it can be an attractive solution for low cost, passive sonar systems.

The incorporation of new piezoelectric materials into sonar systems can be a complex and time-consuming process. This can stem from several factors:

Safety: Sonar systems are often critical to safety as their failure could endanger the platform which it is mounted. Therefore the design approach used in the development of sonar systems usually favour technologies which have been already been demonstrated in operational environments. Meanwhile the adoption of new technologies can be costly and slow due to the need to prove them through expensive and time-consuming acceptance trials. Sonar systems are also expected to operate across different maritime environments which range from -10°C to +50°C. Therefore piezoelectric materials should be able to operate within the range of the temperatures and pressures that are defined by operational requirements of the sonar system without a degradation of performance, and so should be void of any polymorphic phase transitions within these temperatures and pressure.

Legacy systems: Sonar systems are typically designed to be in service for a considerable length of time. This can range from a few years to decades corresponding to the lifespan of the platform which the system is mounted. Nonetheless sonar systems do require maintenance, and this can often involve replacing old sonar transducers with new ones. However the opportunity to retrofit transducers containing new piezoelectric materials can be limited. Components of the sonar system such as the electronics, software, and methods of displaying the sonar image are optimised to process the signal generated by the sonar transducer. Therefore modifying the piezoelectric within a sonar transducer could result in the knock-on effect of complete system redesign which could be commercially or practically unviable.

Commercial: The cost effectiveness and security of supply of a piezoelectric material is considered when designing transducers for sonar systems and products must remain at a competitive price point. As previously mentioned, systems remain in service for a considerable length of time. It is therefore important that materials used in the manufacture of the sonar system are available throughout the lifespan of the sonar product, without a significant drift in their performance of properties. The cost of potential modifications to manufacturing routes should also be considered and therefore preferably be suited to current manufacturing specifications. Materials should also be able to be exposed to elevated temperatures and machining processes carried out during the manufacture of sonar systems. The temperature and period at which piezoelectric materials are exposed to these conditions can vary, however temperatures above 100°C are not uncommon, while materials should also be tough enough to withstand the demands of typical manufacturing processes.

8 Conclusions & Outlook

As some tetragonal single crystals considered in this review have also possess large Curie temperature relative to PZT, the motivation for the growth of piezoelectric single crystal materials such as $BiFeO_3$-$PbTiO_3$ and $Bi(Zn,Ti)O_3$-$PbTiO_3$ will continue to exist and will therefore be an opportunity to provide more piezoelectric property data. Although these systems will be of scientific interest, the ability to grow highly tetragonal crystals on a large scale is questionable and therefore difficult to foresee translation into industry. The significantly high g_{33} values shown for orthorhombic systems, particularly pure and doped $(K,Na)NbO_3$ single crystals, provides an exciting opportunity for fundamental materials scientists, the lead-free and/or single crystal community and device engineers. The successful growth of $(K,Na)NbO_3$ by the modified Bridgman method also demonstrates scalability similar to Generation I, II and III single crystals. However, the fundamental mechanisms that govern this behaviour is still ambiguous and further research is needed. In particular, the construction of a structure-property relation would require a full disclosure of crystallographic properties in both pure orthorhombic and/or pseudo-monoclinic form alongside piezoelectric property data. The growth and characterisation of rhombohedral crystals is likely to expand due to the demand for high d_{ij} materials and therefore g_{ij} data is also expected to be a by-product of this, however similarly to orthorhombic systems, full disclosure of crystallographic properties would be of use in understanding structure-property relations. Texturing may also provide an interesting opportunity and the successful demonstration of enhancing 33-mode and hydrostatic voltage coefficients is an interesting topic for potential incorporation into monolithic hydrophones if demonstrated to be successful in a scalable and cost-effective manner.

With regards to polycrystalline ceramics, there are reports of materials exhibiting g_{33} values larger than those reported for modified PZT and $PbTiO_3$ whilst matching a low-cost agenda. However before these materials can be incorporated into prototype devices, construction of a full piezoelectric property matrix allowing for analysis of hydrostatic properties are imperative. Additional studies such as assessing their ability to cope with the manufacturing and operational demands such as temperature and pressure are also of use. Polycrystalline ceramics have long offered a low-cost, fast-throughput method of analysing the effects of dopants on piezoelectric and dielectric properties compared to single crystal and textured ceramics and will continue to do so. However the effects of d_{ij} may be of more significance in these studies as the enhancement of g_{ij}, particularly for tetragonal systems, may only be realised when inducing translational symmetry through texturing or single crystal growth.

As mentioned previously, composite materials have been the forefront of high g_{ij} piezoelectric materials and have been used to date in relatively niche applications, namely hydrophones and ultrasonic imaging/diagnostic devices. Research to this point has primarily been focussed on

demonstrating improvements in relevant figures of merit and therefore to overcome mistrust of the longevity, research into lifetime properties such as fatigue is critical. Advanced processing methods for forming piezoelectric composites such as freeze casting, 3D printing, and gel casting offer the potential for improvement in terms of cost and a reduction in materials waste over commonly used mature processes, such as dice- and arrange-and-fill. In particular, casting processes are scalable and can be used to produce near-net shape materials, reducing the need for wasteful post-processing required for dice-and-fill materials. The excellent control over microstructure provided by these new processes, particularly printing technologies, could also enable the fabrication of bespoke composites with piezoelectric, dielectric and mechanical properties that are tuned to specific applications and operating conditions, improving performance and lowering the cost of piezocomposites that currently limits their application. Despite most research being primarily focussed on lead-based piezoceramics, the capability to fabricate lead-free composites with bespoke microstructures may also provide interesting opportunities. Although it should be considered that the maximum benefit from forming a composite is realised for piezoelectric materials that exhibit higher dielectric and piezoelectric properties in bulk form.

With the overall piezoelectric device market expected to grow from USD $28.9bn in 2020 to USD $34.7bn in 2025 (+3.7% CAGR) [148], it is likely that the demand for high g_{ij} devices and materials is also expected to grow. Recent developments in piezoelectric composites indicates a growing number of potential applications, particularly as energy harvesting and the internet-of-things related technologies become more mature. Furthermore the reduced mechanical stiffness in these materials could be a method for improving mechanical impedance matching for additional applications beyond hydrophones and medical imaging. Growth in the sonar market is expected to come from the development of unmanned underwater vehicles (UUVs), autonomous underwater vehicles (AUVs) and the autonomous surface vehicles (ASVs) for applications such as oceanographic survey and servicing underwater assets such as oil well installations. Therefore, the demand and development of new piezoelectric materials which exhibit high piezoelectric voltage coefficients provides a plethora of opportunities for collaboration between materials scientists and device engineers in order to offer solutions to systems incorporated on these platforms.

Ultimately it is the individual researcher/research group/industry's agenda, budget and consumer demand which dictates the chemistry and what form these materials take, however it is the hope of the authors that this review may provide a guide to new or established material scientists, and device engineers in industry or academia who may have an interest in high g_{ij} materials.

Acknowledgements

References

1. A. J. Moulson and J. M. Herbert, Electroceramics: materials, properties, applications, John Wiley & Sons, Chichester, 2003
2. C. R. Bowen, V. Y. Topolov and H. A. Kim, Modern piezoelectric energy-harvesting materials, Springer International Publishing, Switzerland, 2016
3. A. Safari and E. K. Akdogan, Piezoelectric and acoustic materials for transducer applications, Springer Science & Business Media, New York, 2008
4. B. Jaffe, W. R. Cook and H. Jaffe, Piezoelectric ceramics, 2nd edition, Academic Press Inc., London, 2012
5. CTS, PZT Materials, Product: 3265HD, Datasheet [online]. Available from: https://www.ctscorp.com/wp-content/uploads/CTS˙-PZT-Materials˙CompleteProperties˙20180829.pdf (Date accessed: 14/08/2020),
6. S. Zhang, F. Li, X. Jiang, J. Kim, J. Luo and X. Geng, Advantages and challenges of relaxor-$PbTiO_3$ ferroelectric crystals for electroacoustic transducers – A review, Progress in materials science **68**[(2015) 1-66. https://doi.org/10.1016/j.pmatsci.2014.10.002
7. S. Zhang and F. Li, High performance ferroelectric relaxor-$PbTiO_3$ single crystals: Status and perspective, Journal of Applied Physics **111**[3] (2012) 031301. https://doi.org/10.1063/1.3679521
8. TRS Technologies, High Performance PMN-PT Piezoelectric Single Crystals, Product: X2B, Datasheet [online]. Available from: http://www.trstechnologies.com/Materials/High-Performance-PMN-PT-Piezoelectric-SingleCrystal (Date accessed: 14/08/2020).
9. E. Sun and W. Cao, Relaxor-based ferroelectric single crystals: growth, domain engineering, characterization and applications, Progress in materials science **65**[(2014) 124-210. https://doi.org/10.1016/j.pmatsci.2014.03.006
10. A. J. Bell, A classical mechanics model for the interpretation of piezoelectric property data, Journal of Applied Physics **118**[22] (2015) 224103. https://doi.org/10.1063/1.4937135
11. A. F. Devonshire, CIX. Theory of barium titanate—Part II, The London, Edinburgh, and Dublin Philosophical Magazine and Journal of Science **42**[333] (1951) 1065-1079. https://doi.org/10.1080/14786445108561354
12. A. F. Devonshire, XCVI. Theory of barium titanate: Part I, The London, Edinburgh, and Dublin Philosophical Magazine and Journal of Science **40**[309] (1949) 1040-1063. https://doi.org/10.1080/14786444908561372
13. M. Davis, M. Budimir, D. Damjanovic and N. Setter, Rotator and extender ferroelectrics: Importance of the shear coefficient to the piezoelectric properties of domain-engineered crystals and ceramics, Journal of Applied Physics **101**[5] (2007) https://doi.org/10.1063/1.2653925
14. J. Koruza, H. Liu, M. Höfling, M.-H. Zhang and P. Veber, $(K,Na)NbO_3$-based piezoelectric single crystals: Growth methods, properties, and applications, Journal of Materials Research **35**[8] (2020) 990-1016. https://doi.org/10.1557/jmr.2019.391
15. H. Tian, C. Hu, X. Meng, P. Tan, Z. Zhou, J. Li, et al., Top-Seeded Solution Growth and Properties of $K_{1−x}Na_xNbO_3$ Crystals, Crystal Growth & Design **15**[3] (2015) 1180-1185. https://doi.org/10.1021/cg501554v
16. F. Li, L. Jin, Z. Xu and S. Zhang, Electrostrictive effect in ferroelectrics: An alternative approach to improve piezoelectricity, Applied Physics Reviews **1**[1] (2014) 011103. https://doi.org/10.1063/1.4861260
17. K. Uchino, S. Nomura, K. Vedam, R. E. Newnham and L. E. Cross, Pressure dependence of the refractive index and dielectric constant in a fluoroperovskite, $KMgF_3$, Physical Review B **29**[12] (1984) 6921. https://doi.org/10.1103/PhysRevB.29.6921
18. C. N. W. Darlington and K. S. Knight, Structural study of potassium niobate between 200K and 823K, Phase Transitions **52**[4] (1994) 261-275. https://doi.org/10.1080/01411599408200379
19. S. Zhang, P. W. Rehrig, C. Randall and T. R. Shrout, Crystal growth and electrical properties of $Pb(Yb_{1/2}Nb_{1/2})O_3$–$PbTiO_3$ perovskite single crystals, Journal of crystal growth **234**[2-3] (2002) 415-420. https://doi.org/10.1016/S0022-0248(01)01696-7

20. A. Kalinichev, J. D. Bass, B. Sun and D. Payne, Elastic properties of tetragonal $PbTiO_3$ single crystals by Brillouin scattering, Journal of Materials Research **12**[10] (1997) 2623-2627. https://doi.org/10.1557/JMR.1997.0349

21. Z. Li, M. Grimsditch, X. Xu and S.-K. Chan, The elastic, piezoelectric and dielectric constants of tetragonal $PbTiO_3$ single crystals, Ferroelectrics **141**[1] (1993) 313-325. https://doi.org/10.1080/00150199308223459

22. M. J. Haun, E. Furman, S. Jang, H. McKinstry and L. Cross, Thermodynamic theory of $PbTiO_3$, Journal of Applied Physics **62**[8] (1987) 3331-3338. https://doi.org/10.1063/1.339293

23. S. Zhang, L. Lebrun, S. Rhee, R. E. Eitel, C. A. Randall and T. R. Shrout, Crystal growth and characterization of new high Curie temperature $(1-x)BiScO_3-xPbTiO_3$ single crystals, Journal of crystal growth **236**[1-3] (2002) 210-216. https://doi.org/10.1016/S0022-0248(01)02093-0

24. S. Zhang, C. A. Randall and T. R. Shrout, Dielectric, piezoelectric and elastic properties of tetragonal $BiScO_3$-$PbTiO_3$ single crystal with single domain, Solid state communications **131**[1] (2004) 41-45. https://doi.org/10.1016/j.ssc.2004.04.016

25. Z. Liu, H. Wu, A. Paterson, Z. Luo, W. Ren and Z.-G. Ye, High Curie-temperature (T_C) piezo-/ferroelectric single crystals with bismuth-based complex perovskites: Growth, structures and properties, Acta Materialia **136**[(2017) 32-38. https://doi.org/10.1016/j.actamat.2017.06.047

26. D. I. Woodward, I. M. Reaney, R. E. Eitel and C. A. Randall, Crystal and domain structure of the $BiFeO_3$–$PbTiO_3$ solid solution, Journal of Applied Physics **94**[5] (2003) 3313-3318. https://doi.org/10.1063/1.1595726

27. A. J. Bell, A. X. Levander, S. L. Turner and T. P. Comyn, Internal stress and phase coexistence in bismuth ferrite-lead titanate ceramics, 2007 Sixteenth IEEE International Symposium on the Applications of Ferroelectrics (2007) 406-409. https://doi.org/10.1109/ISAF.2007.4393280

28. V. V. S. S. S. Sunder, A. Halliyal and A. Umarji, Investigation of tetragonal distortion in the $PbTiO_3$–$BiFeO_3$ system by high-temperature x-ray diffraction, Journal of Materials Research **10**[5] (1995) 1301-1306. https://doi.org/10.1557/JMR.1995.1301

29. S. Bhattacharjee, S. Tripathi and D. Pandey, Morphotropic phase boundary in $(1-x)BiFeO_3$–$xPbTiO_3$: phase coexistence region and unusually large tetragonality, Applied Physics Letters **91**[4] (2007) 042903. https://doi.org/10.1063/1.2766657

30. W.-M. Zhu, H.-Y. Guo and Z.-G. Ye, Structural and magnetic characterization of multiferroic $(BiFeO_3)_{1-x}(PbTiO_3)_x$ solid solutions, Physical Review B **78**[1] (2008) 014401. https://doi.org/10.1103/PhysRevB.78.014401

31. T. Burnett, T. Comyn and A. Bell, Flux growth of $BiFeO_3$–$PbTiO_3$ single crystals, Journal of crystal growth **285**[1-2] (2005) 156-161. https://doi.org/10.1016/j.jcrysgro.2005.08.001

32. W. Zhu, H. Guo and Z. Ye, Structure and properties of multiferroic $(1-x)BiFeO_3$–$xPbTiO_3$ single crystals, Journal of Materials Research **22**[8] (2007) 2136-2143. https://doi.org/10.1557/jmr.2007.0268

33. Innovia Materials, PMN-PT and PIN-PMN-PT Crystal, Webpage [online]. Available from: http://www.innoviamaterials.com/about/?120.html (Date accessed: 27/10/2020),

34. K. Chen, G. Xu, D. Yang, X. Wang and J. Li, Dielectric and piezoelectric properties of lead-free $0.95(K_{0.5}Na_{0.5})NbO_3$–$0.05LiNbO_3$ crystals grown by the Bridgman method, Journal of Applied Physics **101**[4] (2007) 044103. https://doi.org/10.1063/1.2562464

35. D. Lin, Z. Li, F. Li, C. Cai, W. Liu and S. Zhang, Tetragonal-to-tetragonal phase transition in lead-free $(K_xNa_{1-x})NbO_3$ (x= 0.11 and 0.17) crystals, Crystals **4**[2] (2014) 113-122. https://doi.org/10.3390/cryst4020113

36. Biotain, Barium Titanate ($BaTiO_3$) Single Crystal, Webpage [online]. Available from: http://www.crystal-material.com/Single-Crystal-Materials/Bariumtitanate-BaTiO3-single-crystal.html (Date accessed: 17/01/2020),

37. MaTecK, $BaTiO_3$ - Barium Titanate Crystal, Webpage [online]. Available from: https://mateck.com/info/batio3-barium-titanate-crystal.html (Date accessed: 17/01/2020),

38. MTI Corporation, $BaTiO_3$ (001) 5x5x1mm, 1SP, Substrate Grade, Item number: BTOb050510S1SDUS, Webpage [online]. Available from: https://www.mtixtl.com/BTO-b-050510-S1-1.aspx (Date accessed: 27/10/2020),

39. L. Levinson, Electronic Ceramics: Properties: Devices, and Applications, Marcel Dekker Inc., New York, 1988

40. M. Sharma, H. Sharma and K. Raina, Comparison of piezoelectricity in Ta^{5+} and La^{3+} substituted lead calcium titanate ceramics, Journal of Physics and Chemistry of Solids **69**[10] (2008) 2584-2588. https://doi.org/10.1016/j.jpcs.2008.05.019

41. S. Singh, C. Prakash and K. Raina, Microstructure and electron properties of Sm modified lead calcium titanate ceramics, Journal of alloys and compounds **492**[1-2] (2010) 717-722. https://doi.org/10.1016/j.jallcom.2009.12.025

42. L. M. Troilo, D. Damjanovic and R. E. Newnham, Modified lead calcium titanate ceramics with a relatively large dielectric constant for hydrophone applications, Journal of the American Ceramic Society **77**[3] (1994) 857-859. https://doi.org/10.1111/j.1151-2916.1994.tb05380.x

43. Y. Yamashita, K. Yokoyama, H. Honda and T. Takahashi, $(Pb,Ca)((Co_{1/2}W_{1/2}),Ti)O_3$ piezoelectric ceramics and their applications, Japanese Journal of Applied Physics **20**[S4] (1981) 183. https://doi.org/10.7567/JJAPS.20S4.183

44. D. Garcia and J. Eiras, Piezoelectric and dielectric properties of some La, Mn modified $PbTiO_3$ ceramics, Ferroelectrics **123**[1] (1991) 51-59. https://doi.org/10.1080/00150199108244712

45. I. Ueda and S. Ikegami, Piezoelectric properties of modified $PbTiO_3$ ceramics, Japanese Journal of Applied Physics **7**[3] (1968) 236-242. https://doi.org/10.1143/JJAP.7.236

46. S. Singh, O. Thakur, C. Prakash and K. Raina, Structural and electrical properties of lanthanum-substituted lead titanate ceramics, Phase Transitions **78**[7-8] (2005) 655-667. https://doi.org/10.1080/01411590500271235

47. J. F. Li, K. Wang, F. Y. Zhu, L. Q. Cheng and F. Z. Yao, $(K,Na)NbO_3$- based lead- free piezoceramics: fundamental aspects, processing technologies, and remaining challenges, Journal of the American Ceramic Society **96**[12] (2013) 3677-3696. https://doi.org/10.1111/jace.12715

48. S. Dwivedi, T. Pareek, M. Badole, S. A. Ahmed and S. Kumar, Effects of $LaScO_3$ doping on structure, dielectric, and piezoelectric properties of $K_{0.5}Na_{0.5}NbO_3$ piezoceramics, Journal of Applied Physics **127**[9] (2020) 094104. https://doi.org/10.1063/1.5141530

49. N. Luo, Q. Li and Z. Xia, Effect of $Pb(Fe_{1/2}Nb_{1/2})O_3$ modification on dielectric and piezoelectric properties of $Pb(Mg_{1/3}Nb_{2/3})O_3$–$PbZr_{0.52}Ti_{0.48}O_3$ ceramics, Materials Research Bulletin **46**[9] (2011) 1333-1339. https://doi.org/10.1016/j.materresbull.2011.05.026

50. H. Tao, J. Lv, R. Zhang, R. Xiang and J. Wu, Lead-free rare earth-modified $BiFeO_3$ ceramics: phase structure and electrical properties, Materials & Design **120**[(2017) 83-89. https://doi.org/10.1016/j.matdes.2017.01.083

51. M. A. Carpenter, E. K. H. Salje and A. Graeme-Barber, Spontaneous strain as a determinant of thermodynamic properties for phase transitions in minerals, European Journal of Mineralogy **10**[4] (1998) 621-691. https://doi.org/10.1127/ejm/10/4/0621

52. C.-W. Ahn, G. Han, J. Ryu, W.-H. Yoon, J.-J. Choi, B.-D. Hahn, et al., Composition design rule for high piezoelectric voltage coefficient in $(K_{0.5}Na_{0.5})NbO_3$ based Pb-free ceramics, Japanese Journal of Applied Physics **51**[9S2] (2012) 09MD10. https://doi.org/10.1143/JJAP.51.09MD10

53. T. E. Hooper, High Voltage Coefficient Piezoelectric Materials For Underwater Transducer Applications, PhD thesis, University of Leeds, 2020

54. T. Leist, T. Granzow, W. Jo and J. Rödel, Effect of tetragonal distortion on ferroelectric domain switching: a case study on La-doped $BiFeO_3$–$PbTiO_3$ ceramics, Journal of Applied Physics **108**[1] (2010) 014103. https://doi.org/10.1063/1.3445771

55. Z. Li, H. Yang, H. Tian, J. Li, J. Cheng and J. Chen, Transmission electron microscopy study of multiferroic $(Bi_{1-x}La_x)FeO_3$–$PbTiO_3$ with x= 0.1, 0.2, and 0.3, Applied Physics Letters **90**[18] (2007) 182904. https://doi.org/10.1063/1.2735553

56. S.-H. Yoon, M.-Y. Kim and D. Kim, Influence of tetragonality (c/a) on dielectric nonlinearity and direct current (dc) bias characteristics of $(1-x)BaTiO_3$-$xBi_{0.5}Na_{0.5}TiO_3$ ceramics, Journal of Applied Physics **122**[15] (2017) 154103. https://doi.org/10.1063/1.5000019

57. G. Tutuncu, B. Li, K. Bowman and J. L. Jones, Domain wall motion and electromechanical strain in lead-free piezoelectrics: Insight from the model system $(1-x)Ba(Zr_{0.2}Ti_{0.8})O_3$–$x(Ba_{0.7}Ca_{0.3})TiO_3$

using in situ high-energy X-ray diffraction during application of electric fields, Journal of Applied Physics **115**[14] (2014) 144104. https://doi.org/10.1063/1.4870934

58. Z. Peng, Q. Chen, D. Yan, D. Xiao and J. Zhu, Characterization of potassium-modified $Li_{0.12}Na_{0.88}Nb_{0.97}Sb_{0.03}O_3$ lead-free piezoceramics, Journal of alloys and compounds **582**[(2014) 834-838. https://doi.org/10.1016/j.jallcom.2013.08.111

59. B. Liu, P. Li, B. Shen, J. Zhai, Y. Zhang, F. Li, et al., Simultaneously enhanced piezoelectric response and piezoelectric voltage coefficient in textured KNN-based ceramics, Journal of the American Ceramic Society **101**[1] (2018) 265-273. https://doi.org/10.1111/jace.15175

60. Y. Liu, Y. Chang, E. Sun, F. Li, S. Zhang, B. Yang, et al., Significantly enhanced energy-harvesting performance and superior fatigue-resistant behavior in [001]c-textured $BaTiO_3$-based lead-free piezoceramics, ACS applied materials & interfaces **10**[37] (2018) 31488-31497. https://doi.org/10.1021/acsami.8b10361

61. Y. Yan, J. E. Zhou, D. Maurya, Y. U. Wang and S. Priya, Giant piezoelectric voltage coefficient in grain-oriented modified $PbTiO_3$ material, Nature communications **7**[1] (2016) 13089. https://doi.org/10.1038/ncomms13089

62. Y. Yan, K.-H. Cho, D. Maurya, A. Kumar, S. Kalinin, A. Khachaturyan, et al., Giant energy density in [001]-textured $Pb(Mg_{1/3}Nb_{2/3})O_3$-$PbZrO_3$-$PbTiO_3$ piezoelectric ceramics, Applied Physics Letters **102**[4] (2013) 042903. https://doi.org/10.1063/1.4789854

63. Y. Chang, S. Poterala, Z. Yang and G. L. Messing, Enhanced Electromechanical Properties and Temperature Stability of Textured $(K_{0.5}Na_{0.5})NbO_3$- Based Piezoelectric Ceramics, Journal of the American Ceramic Society **94**[8] (2011) 2494-2498. https://doi.org/10.1111/j.1551-2916.2011.04393.x

64. R. Newnham, D. Skinner and L. Cross, Connectivity and piezoelectric-pyroelectric composites, Materials Research Bulletin **13**[5] (1978) 525-536. https://doi.org/10.1016/0025-5408(78)90161-7

65. E. K. Akdogan, M. Allahverdi and A. Safari, Piezoelectric composites for sensor and actuator applications, IEEE transactions on ultrasonics, ferroelectrics, and frequency control **52**[5] (2005) 746-775. https://doi.org/10.1109/tuffc.2005.1503962

66. J. Roscow, Y. Zhang, J. Taylor and C. Bowen, Porous ferroelectrics for energy harvesting applications, The European Physical Journal Special Topics **224**[14-15] (2015) 2949-2966. https://doi.org/10.1140/epjst/e2015-02600-y

67. A. N. Rybyanets, Porous piezoceramics: theory, technology, and properties, IEEE transactions on ultrasonics, ferroelectrics, and frequency control **58**[7] (2011) 1492-1507. https://doi.org/10.1109/TUFFC.2011.1968

68. H. Kara, R. Ramesh, R. Stevens and C. R. Bowen, Porous PZT ceramics for receiving transducers, IEEE transactions on ultrasonics, ferroelectrics, and frequency control **50**[3] (2003) 289-296. https://doi.org/10.1109/tuffc.2003.1193622

69. K. Klicker, W. Schulze and J. Biggers, Piezoelectric composites with 3–1 connectivity and a foamed polyurethane matrix, Journal of the American Ceramic Society **65**[12] (1982) 208-210. https://doi.org/10.1111/j.1151-2916.1982.tb09953.x

70. C. Bowen and V. Y. Topolov, Piezoelectric sensitivity of $PbTiO_3$-based ceramic/polymer composites with 0–3 and 3–3 connectivity, Acta Materialia **51**[17] (2003) 4965-4976. https://doi.org/10.1016/s1359-6454(03)00283-0

71. E. Roncari, C. Galassi, F. Craciun, C. Capiani and A. Piancastelli, A microstructural study of porous piezoelectric ceramics obtained by different methods, Journal of the European Ceramic Society **21**[3] (2001) 409-417. https://doi.org/10.1016/S0955-2219(00)00208-9

72. C. Bowen, A. Perry, A. Lewis and H. Kara, Processing and properties of porous piezoelectric materials with high hydrostatic figures of merit, Journal of the European Ceramic Society **24**[2] (2004) 541-545. https://doi.org/10.1016/S0955-2219(03)00194-8

73. E. Mercadelli, A. Sanson and C. Galassi, Porous piezoelectric ceramics, in: E. Suaste-Gomez, Piezoelectric Ceramics, InTech Open Access Publisher, Rijeka, 2010, 111-128

74. C. Galassi, Processing of porous ceramics: Piezoelectric materials, Journal of the European Ceramic Society **26**[14] (2006) 2951-2958. https://doi.org/10.1016/j.jeurceramsoc.2006.02.011

75. A. Safari and E. Akdogan, Rapid prototyping of novel piezoelectric composites, Ferroelectrics **331**[1] (2006) 153-179. https://doi.org/10.1080/00150190600737727

76. H. Cui, R. Hensleigh, D. Yao, D. Maurya, P. Kumar, M. G. Kang, et al., Three-dimensional printing of piezoelectric materials with designed anisotropy and directional response, Nature materials **18**[3] (2019) 234-241. https://doi.org/10.1038/s41563-018-0268-1

77. L. Shu, R. Liang, Y. Yu, T. Tian, Z. Rao and Y. Wang, Unique elastic, dielectric and piezoelectric properties of micro-architected metamaterials, Journal of Materials Chemistry C **7**[9] (2019) 2758-2765. https://doi.org/10.1039/C8TC05847D

78. A. Safari, R. E. Newnham, L. E. Cross and W. A. Schulze, Perforated PZT-polymer composites for piezoelectric transducer applications, Ferroelectrics **41**[1] (1982) 197-205. https://doi.org/10.1080/00150198208210624

79. R. W. Lewis, A. C. Dent, R. Stevens and C. R. Bowen, Microstructural modelling of the polarization and properties of porous ferroelectrics, Smart materials and structures **20**[8] (2011) 085002. https://doi.org/10.1088/0964-1726/20/8/085002

80. J. Roscow, R. Lewis, J. Taylor and C. Bowen, Modelling and fabrication of porous sandwich layer barium titanate with improved piezoelectric energy harvesting figures of merit, Acta Materialia **128**[(2017) 207-217. https://doi.org/10.1016/j.actamat.2017.02.029

81. Y. Zhang, J. Roscow, R. Lewis, H. Khanbareh, V. Y. Topolov, M. Xie, et al., Understanding the effect of porosity on the polarisation-field response of ferroelectric materials, Acta Materialia **154**[(2018) 100-112. https://doi.org/10.1016/j.actamat.2018.05.007

82. J. Roscow, Y. Zhang, M. Kraśny, R. Lewis, J. Taylor and C. Bowen, Freeze cast porous barium titanate for enhanced piezoelectric energy harvesting, Journal of Physics D: Applied Physics **51**[22] (2018) 225301. https://doi.org/10.1088/1361-6463/aabc81

83. F. Bouville, E. Portuguez, Y. Chang, G. L. Messing, A. J. Stevenson, E. Maire, et al., Templated grain growth in macroporous materials, Journal of the American Ceramic Society **97**[6] (2014) 1736-1742. https://doi.org/10.1111/jace.12976

84. S. H. Lee, S. H. Jun, H. E. Kim and Y. H. Koh, Piezoelectric properties of PZT-based ceramic with highly aligned pores, Journal of the American Ceramic Society **91**[6] (2008) 1912-1915. https://doi.org/10.1111/j.1551-2916.2008.02359.x

85. J. Schultheiß, J. I. Roscow and J. Koruza, Orienting anisometric pores in ferroelectrics: Piezoelectric property engineering through local electric field distributions, Physical Review Materials **3**[8] (2019) 084408. https://doi.org/10.1103/PhysRevMaterials.3.084408

86. D. P. Skinner, R. E. Newnham and L. E. Cross, Flexible composite transducers, Materials Research Bulletin **13**[6] (1978) 577-607. https://doi.org/10.1016/0025-5408(78)90185-X

87. K. Rittenmyer, T. Shrout, W. A. Schulze and R. E. Newnham, Piezoelectric 3–3 composites, Ferroelectrics **41**[1] (1982) 189-195. https://doi.org/10.1080/00150198208210623

88. S.-H. Lee, S.-H. Jun, H.-E. Kim and Y.-H. Koh, Fabrication of porous PZT–PZN piezoelectric ceramics with high hydrostatic figure of merits using camphene-based freeze casting, Journal of the American Ceramic Society **90**[9] (2007) 2807-2813. https://doi.org/10.1111/j.1551-2916.2007.01834.x

89. K. A. Klicker, J. V. Biggers and R. E. Newnham, Composites of PZT and epoxy for hydrostatic transducer applications, Journal of the American Ceramic Society **64**[1] (1981) 5-9. https://doi.org/10.1111/j.1151-2916.1981.tb09549.x

90. Y. Zhang, J. Roscow, M. Xie and C. Bowen, High piezoelectric sensitivity and hydrostatic figures of merit in unidirectional porous ferroelectric ceramics fabricated by freeze casting, Journal of the European Ceramic Society **38**[12] (2018) 4203-4211. https://doi.org/10.1016/j.jeurceramsoc.2018.04.067

91. T. L. Szabo, Diagnostic Ultrasound Imaging: Inside Out, 2nd edition, Academic Press, Oxford, 2013

92. J. L. Butler and C. H. Sherman, Transducers and arrays for underwater sound, 2nd edition, Springer International Publishing, Switzerland, 2016

93. I. Katsouras, K. Asadi, M. Li, T. B. van Driel, K. S. Kjaer, D. Zhao, et al., The negative piezoelectric effect of the ferroelectric polymer poly(vinylidene fluoride), Nature materials **15**[1] (2016) 78-84. https://doi.org/10.1038/nmat4423

94. T. Furukawa, Piezoelectricity and pyroelectricity in polymers, IEEE Transactions on Electrical Insulation **24**[3] (1989) 375–394. https://doi.org/10.1109/14.30878

95. H. Kawai, The piezoelectricity of poly(vinylidene fluoride), Japanese Journal of Applied Physics **8**[7] (1969) 975. https://doi.org/10.1143/JJAP.8.975

96. E. Yamaka, Pyroelectric IR sensor using vinylidene fluoride-trifluoroethylene copolymer film, Ferroelectrics **57**[1] (1984) 337-342. https://doi.org/10.1080/00150198408012772

97. T. Kitayama and S. Sugawara, Piezoelectric and pyroelectric properties of polymer ferroelectric composites., Professional Report Gr. Inst. Elec. Comm. Eng. Japan (1972) CPM72.

98. A. Pelaiz-Barranco and P. Marin-Franch, Piezo-, pyro-, ferro-, and dielectric properties of ceramic/polymer composites obtained from two modifications of lead titanate, Journal of Applied Physics **97**[3] (2005) 034104. https://doi.org/10.1063/1.1847727

99. J.-H. Seol, J. S. Lee, H.-N. Ji, Y.-P. Ok, G. P. Kong, K.-S. Kim, et al., Piezoelectric and dielectric properties of $(K_{0.44}Na_{0.52}Li_{0.04})(Nb_{0.86}Ta_{0.10}Sb_{0.04})O_3$–PVDF composites, Ceramics International **38**[(2012) S263-S266. https://doi.org/10.1016/j.ceramint.2011.04.097

100. H. Banno and S. Saito, Piezoelectric and dielectric properties of composites of synthetic rubber and $PbTiO_3$ or PZT, Japanese Journal of Applied Physics **22**[S2] (1983) 67. https://doi.org/10.7567/JJAPS.22S2.67

101. T. Yamada, T. Ueda and T. Kitayama, Piezoelectricity of a high-content lead zirconate titanate/polymer composite, Journal of Applied Physics **53**[6] (1982) 4328-4332. https://doi.org/10.1063/1.331211

102. G. Sa-Gong, A. Safari, S. J. Jang and R. E. Newnham, Poling flexible piezoelectric composites, Ferroelectrics Letters Section **5**[5] (1986) 131-142. https://doi.org/10.1080/07315178608202472

103. C. Dias, D. K. Das-Gupta, Y. Hinton and R. J. Shuford, Polymer/ceramic composites for piezoelectric sensors, Sensors and Actuators A: Physical **37**[(1993) 343-347. https://doi.org/10.1016/0924-4247(93)80058-O

104. D. T. Le, N. B. Do, D. U. Kim, I. Hong, I.-W. Kim and J. S. Lee, Preparation and characterization of lead-free $(K_{0.47}Na_{0.51}Li_{0.02})(Nb_{0.8}Ta_{0.2})O_3$ piezoceramic/epoxy composites with 0–3 connectivity, Ceramics International **38**[1] (2012) S259-S262. https://doi.org/10.1016/j.ceramint.2011.04.096

105. K. A. Klicker, Piezoelectric Composites with 3-1 Connectivity for Transducer Applications, PhD thesis, Pennsylvania State University, 1981

106. H. P. Savakus, K. A. Klicker and R. E. Newnham, PZT-epoxy piezoelectric transducers: a simplified fabrication procedure, Materials Research Bulletin **16**[6] (1981) 677-680. https://doi.org/10.1016/0025-5408(81)90267-1

107. C. P. Bowen, R. E. Newnham and C. A. Randall, Dielectric properties of dielectrophoretically assembled particulate-polymer composites, Journal of Materials Research **13**[1] (1998) 205-210. https://doi.org/10.1557/JMR.1998.0027

108. S. A. Wilson, G. M. Maistros and R. W. Whatmore, Structure modification of 0–3 piezoelectric ceramic/polymer composites through dielectrophoresis, Journal of Physics D: Applied Physics **38**[2] (2005) 175. https://doi.org/10.1088/0022-3727/38/2/001

109. H. Khanbareh, S. v. d. Zwaag and W. A. Groen, Effect of dielectrophoretic structuring on piezoelectric and pyroelectric properties of lead titanate-epoxy composites, Smart materials and structures **23**[10] (2014) 105030. https://doi.org/10.1088/0964-1726/23/10/105030

110. D. B. Deutz, N. T. Mascarenhas, S. van der Zwaag and W. A. Groen, Enhancing energy harvesting potential of $(K,Na,Li)NbO_3$-epoxy composites via Li substitution, Journal of the American Ceramic Society **100**[3] (2017) 1108-1117. https://doi.org/10.1111/jace.14698

111. D. B. Deutz, N. T. Mascarenhas, J. B. J. Schelen, D. M. de Leeuw, S. van der Zwaag and P. Groen, Flexible piezoelectric touch sensor by alignment of lead-free alkaline niobate microcubes in PDMS, Advanced Functional Materials **27**[24] (2017) 1700728. https://doi.org/10.1002/adfm.201700728

112. N. K. James, D. B. Deutz, R. K. Bose, S. v. d. Zwaag and P. Groen, High piezoelectric voltage coefficient in structured lead-free (K,Na,Li)NbO$_3$ particulate—epoxy composites, Journal of the American Ceramic Society **99**[12] (2016) 3957-3963. https://doi.org/10.1111/jace.14428

113. D. A. van den Ende, B. F. Bory, W. A. Groen and S. van der Zwaag, Improving the d$_{33}$ and g$_{33}$ properties of 0-3 piezoelectric composites by dielectrophoresis, Journal of Applied Physics **107**[2] (2010) 024107. https://doi.org/10.1063/1.3291131

114. H. Khanbareh, S. van der Zwaag and W. A. Groen, In-situ poling and structurization of piezoelectric particulate composites, Journal of Intelligent Material Systems and Structures **28**[18] (2017) 2467-2472. https://doi.org/10.1177/1045389X17689928

115. H. Khanbareh, K. de Boom, B. Schelen, R. Scharff, C. Wang, S. van der Zwaag, et al., Large area and flexible micro-porous piezoelectric materials for soft robotic skin, Sensors and Actuators A: Physical **263**[(2017) 554-562. https://doi.org/10.1016/j.sna.2017.07.001

116. D. A. v. d. Ende, W. A. Groen and S. v. d. Zwaag, Robust piezoelectric composites for energy harvesting in high-strain environments, Journal of Intelligent Material Systems and Structures **24**[18] (2013) 2262-2269. https://doi.org/10.1177/1045389X12462646

117. M. A. Gutíerrez, H. Khanbareh and S. v. d. Zwaag, Computational modelling of structure formation during dielectrophoresis in particulate composites, Computational Materials Science **112**[(2016) 139-146. https://doi.org/10.1016/j.commatsci.2015.10.011

118. D. B. Deutz, N. T. Mascarenhas, S. van der Zwaag and W. A. Groen, Poling piezoelectric (K,Na,Li)NbO$_3$-polydimethylsiloxane composites, Ferroelectrics **515**[1] (2017) 68-74. https://doi.org/10.1143/JJAP.46.7089

119. S. E. v. Kempen, H. Khanbareh, P. Groen, J. M. A. M. Hol and S. v. d. Zwaag, Effect of topological imperfections on the electro-mechanical properties of structured piezoelectric particulate composites, Journal of Physics: Materials **3**[1] (2019) 014004. https://doi.org/10.1088/2515-7639/ab50f8

120. V. L. Stuber, D. B. Deutz, J. Bennett, D. Cannel, D. M. d. Leeuw, S. v. d. Zwaag, et al., Flexible lead-free piezoelectric composite materials for energy harvesting applications, Energy Technology **7**[1] (2019) 177-185. https://doi.org/10.1002/ente.201800419

121. C. Dagdeviren, P. Joe, O. L. Tuzman, K.-I. Park, K. J. Lee, Y. Shi, et al., Recent progress in flexible and stretchable piezoelectric devices for mechanical energy harvesting, sensing and actuation, Extreme Mechanics Letters **9**[1] (2016) 269-281. https://doi.org/10.1016/j.eml.2016.05.015

122. Y. Zhang and M. Lu, A review of recent advancements in soft and flexible robots for medical applications, The International Journal of Medical Robotics and Computer Assisted Surgery **16**[3] (2020) e2096. https://doi.org/10.1002/rcs.2096

123. M. Amjadi, K.-U. Kyung, I. Park and M. Sitti, Stretchable, skin-mountable, and wearable strain sensors and their potential applications: a review, Advanced Functional Materials **26**[11] (2016) 1678-1698. https://doi.org/10.1002/adfm.201504755

124. D. Stansfield and A. Elliott, Underwater Electroacoustic Transducers, 2nd edition, Peninsula Publishing, Los Altos, 2017

125. J. Dargahi and S. Najarian, Advances in tactile sensors design/manufacturing and its impact on robotics applications–a review, Industrial Robot **32**[3] (2005) 268-281. https://doi.org/10.1108/01439910510593965

126. I. Graz, M. Krause, S. Bauer-Gogonea, S. Bauer, S. P. Lacour, B. Ploss, et al., Flexible active-matrix cells with selectively poled bifunctional polymer-ceramic nanocomposite for pressure and temperature sensing skin, Journal of Applied Physics **106**[3] (2009) 034503. https://doi.org/10.1063/1.3191677

127. J. H. Lee, H. J. Yoon, T. Y. Kim, M. K. Gupta, J. H. Lee, W. Seung, et al., Micropatterned P(VDF-TrFE) film- based piezoelectric nanogenerators for highly sensitive self-powered pressure sensors, Advanced Functional Materials **25**[21] (2015) 3203-3209. https://doi.org/10.1002/adfm.201500856

128. H. Montazerian, A. Rashidi, A. S. Milani and M. Hoorfar, Integrated sensors in advanced composites: A critical review, Critical Reviews in Solid State and Materials Sciences **45**[3] (2020) 187-238. https://doi.org/10.1080/10408436.2019.1588705

129. S. Bauer, S. Bauer-Gogonea, I. Graz, M. Kaltenbrunner, C. Keplinger and R. Schwodiauer, 25th anniversary article: A soft future: from robots and sensor skin to energy harvesters, Advanced Materials **26**[1] (2014) 149-161. https://doi.org/10.1002/adma.201303349

130. M. L. Hammock, A. Chortos, B. C. Tee, J. B. Tok and Z. Bao, 25th anniversary article: The evolution of electronic skin (e-skin): a brief history, design considerations, and recent progress, Adv Mater **25**[42] (2013) 5997-6038. https://doi.org/10.1002/adma.201302240

131. G. Scheipl, M. Zirkl, A. Sawatdee, U. Helbig, M. Krause, E. Kraker, et al., All printed touchless human-machine interface based on only five functional materials, Organic Photonic Materials and Devices XIV 8258[(2012) 82580P. https://doi.org/10.1117/12.908602

132. M. Ha, S. Lim, J. Park, D.-S. Um, Y. Lee and H. Ko, Bioinspired interlocked and hierarchical design of ZnO nanowire arrays for static and dynamic pressure-sensitive electronic skins, Advanced Functional Materials **25**[19] (2015) 2841-2849. https://doi.org/10.1002/adfm.201500453

133. M. Zirkl, A. Sawatdee, U. Helbig, M. Krause, G. Scheipl, E. Kraker, et al., An all-printed ferroelectric active matrix sensor network based on only five functional materials forming a touchless control interface, Advanced Materials **23**[18] (2011) 2069-2074. https://doi.org/10.1002/adma.201100054

134. K. Uchino, Piezoelectric energy harvesting systems—Essentials to successful developments, Energy Technology **6**[5] (2018) 829-848. https://doi.org/10.1002/ente.201700785

135. C. Bowen, H. Kim, P. Weaver and S. Dunn, Piezoelectric and ferroelectric materials and structures for energy harvesting applications, Energy & Environmental Science **7**[1] (2014) 25-44. https://doi.org/10.1039/c3ee42454e

136. M. Safaei, H. A. Sodano and S. R. Anton, A review of energy harvesting using piezoelectric materials: state-of-the-art a decade later (2008–2018), Smart materials and structures **28**[11] (2019) 10.1088/1361-665X/ab36e4

137. R. A. Islam and S. Priya, Realization of high-energy density polycrystalline piezoelectric ceramics, Applied Physics Letters **88**[3] (2006) 032903. https://doi.org/10.1063/1.2166201

138. J. I. Roscow, H. Pearce, H. Khanbareh, S. Kar-Narayan and C. R. Bowen, Modified energy harvesting figures of merit for stress-and strain-driven piezoelectric systems, The European Physical Journal Special Topics **228**[7] (2019) 1537-1554. https://doi.org/10.1140/epjst/e2019-800143-7

139. Smart Materials, Webpage [online]. Available from: https://www.smart-material.com/index.html (Date accessed: 27/10/2020),

140. K. A. Cunefare, E. A. Skow, A. Erturk, J. Savor, N. Verma and M. R. Cacan, Energy harvesting from hydraulic pressure fluctuations, Smart materials and structures **22**[2] (2013) 025036. https://doi.org/10.1088/0964-1726/22/2/025036

141. F. T. Calkins, R. C. Smith and A. B. Flatau, An energy-based hysteresis model for magnetostrictive transducers, IEEE Transactions on Magnetics 36[2] (2000) 429-439. https://doi.org/10.1109/20.825804

142. W. Wang and P. J. Thomas, Low-frequency active noise control of an underwater large-scale structure with distributed giant magnetostrictive actuators, Sensors and Actuators A: Physical **263**[(2017) 113-121. https://doi.org/10.1016/j.sna.2017.05.044

143. R. Bogue, Fibre optic sensors: a review of today's applications, Sensor Review **31**[4] (2011) 304-309. https://doi.org/10.1108/02602281111169703

144. W. Weise, V. Wilkens and C. Koch, Frequency response of fiber-optic multilayer hydrophones: experimental investigation and finite element simulation, IEEE transactions on ultrasonics, ferroelectrics, and frequency control **49**[7] (2002) 937-946. https://doi.org/10.1109/TUFFC.2002.1020164

145. C. K. Kirkendall and A. Dandridge, Overview of high performance fibre-optic sensing, Journal of Physics D: Applied Physics **37**[18] (2004) R197. https://doi.org/10.1088/0022-3727/37/18/R01

146. *Military Standard, Piezoelectric ceramic material and measurements guidelines for sonar transducers, MILSTD-1376B*. 24th February 1995.

147. G. Hayward, J. Bennett and R. Hamilton, A theoretical study on the influence of some constituent material properties on the behavior of 1-3 connectivity composite transducers, The Journal of the Acoustical Society of America **98**[4] (1995) 2187-2196. https://doi.org/10.1121/1.413333

148. Markets and Markets, Piezoelectric Devices Market, Webpage [online]. Available from: https://www.marketsandmarkets.com/PressReleases/piezoelectric-devices.asp (Date accessed: 27/10/2020). https://www.marketsandmarkets.com/PressReleases/piezoelectric-devices.asp,

High Voltage Coefficient Piezoelectric Materials and Their Applications: Supplementary Graphs

Thomas E. Hooper[a1], James. I. Roscow[b], Andrew Mathieson[c], Hamideh Khanbareh[b], Anton J. Goetzee-Barral[a] & Andrew J. Bell[a]

[a]School of Chemical and Process Engineering, University of Leeds, Leeds LS2 9JT, UK
[b]Department of Mechanical Engineering, University of Bath, Bath BA1 9BJ, UK
[c]Ultra Maritime Systems, Dartmouth, Nova Scotia Canada, B2Y 4N2

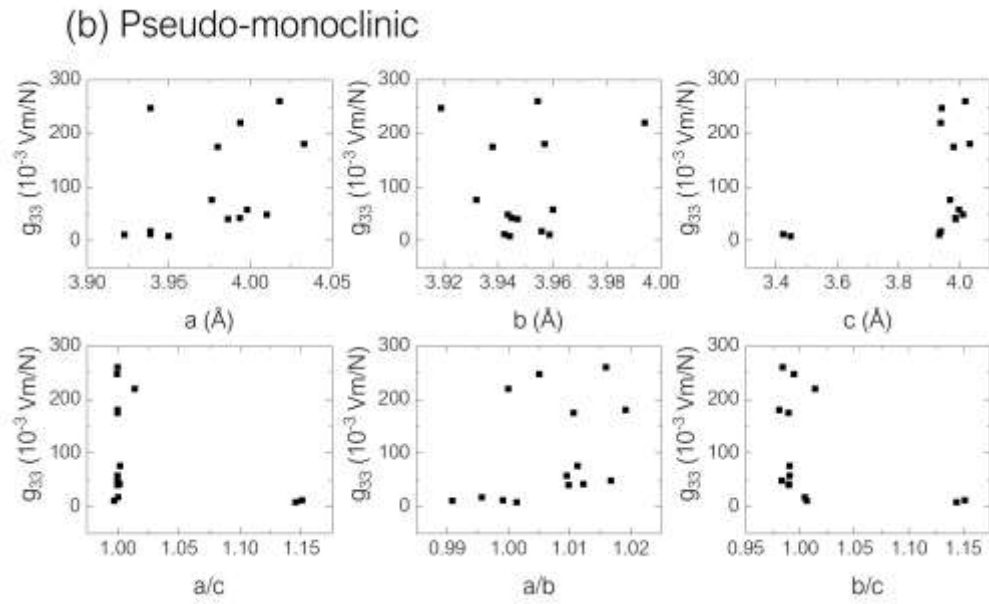## A   Orthorhombic Single Crystals

(a) Pure orthorhombic
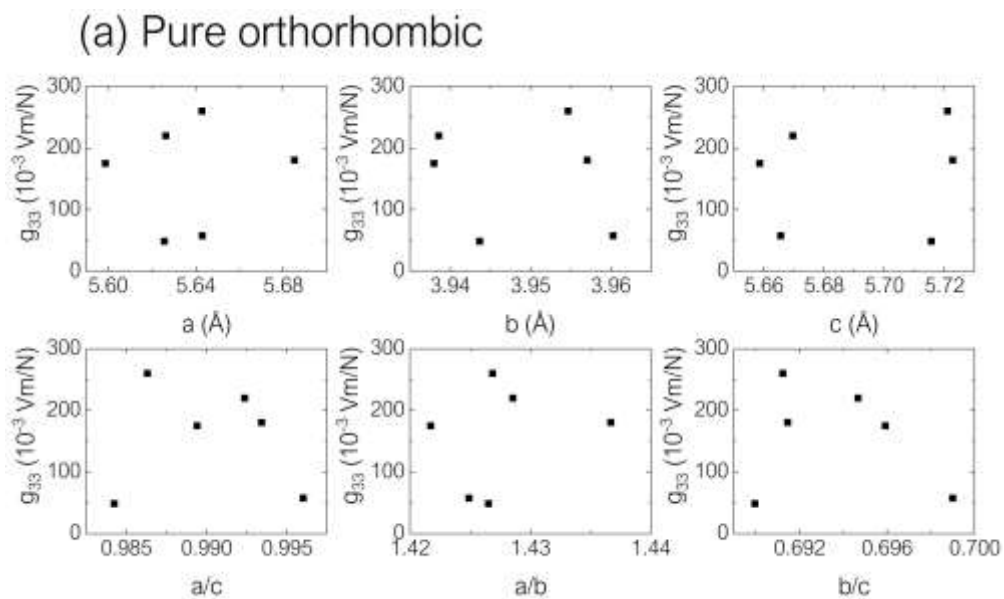
Figure 1: Piezoelectric g_{33} coefficient versus individual orthorhombic lattice parameters and lattice parameter ratios in the (a) pure orthorhombic, and (b) pseudo-monoclinic context.
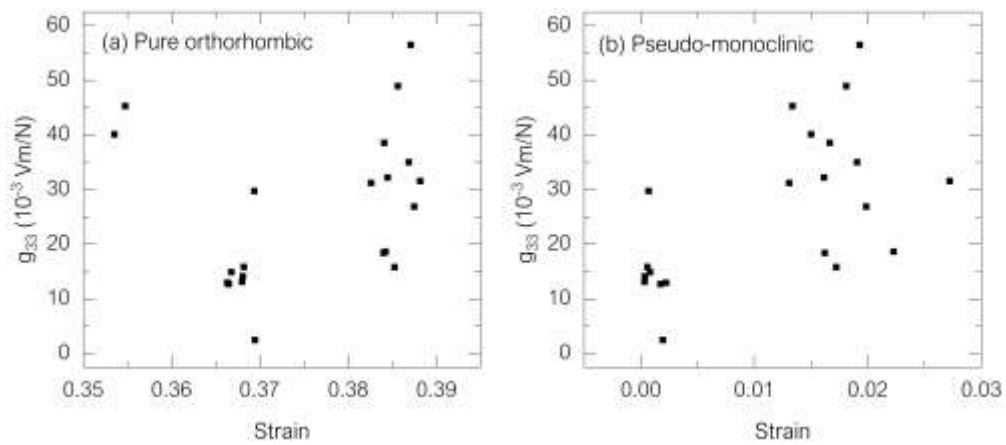

Figure 2: Piezoelectric g_{33} coefficient versus individual orthorhombic lattice parameters and lattice parameter ratios in the (a) pure orthorhombic, and (b) pseudo-monoclinic context.